Shear-reversible clusters of HIV-1 in solution: stabilized by antibodies, dispersed by mucin

Ayobami I Ogundiran[1], Tzu-Lan Chang[1], Andrey Ivanov[2], Namita Kumari[2,3], Sergei Nekhai[2,3], Preethi L. Chandran[1]

[1] Department of Chemical Engineering, College of Engineering and Architecture

[2] Center for Sickle Cell Disease, College of Medicine

[3] Department of Medicine, College of Medicine

Howard University, Washington DC

Corresponding author

Preethi L. Chandran, PhD

Associate Professor

Department of Chemical Engineering, College of Engineering and Architecture, Howard University

Address:

1011 LK Downing Hall

2300 6th Street, NW, Howard University

Washington, DC 20059.

Email: preethi.chandran@howard.edu

Phone: 202-806-4595

Keywords:
HIV, VSV G glycoprotein, gp120, glycosylation, viral aggregation, virus, Dynamic Light Scattering, AFM, high mannose, lectin, mucin

Abstract

HIV-1 has eluded vaccine therapy for the past 40 years. The virus mutates rapidly and is protected by a shifting glycan shield of mannose sugars, which has hindered the broad neutralization of the virus by antibodies (Ab). Studies have shown that mannose residues are self-adhesive, but it is not known if these adhesions drive HIV-1 to aggregate in solution, further complicating Ab neutralization. The behavior of HIV-1 in culture media was monitored using Dynamic Light Scattering (DLS) and complementary atomic force microscopy (AFM) imaging in the presence of anti-gp120 Abs, lectins, mannosidase, and mucin. After accounting for the serum contribution from the culture media, HIV-1 was found to be diffusing in solution in 400-700 nm clusters. These clusters could be sheared into single virus particles by filtration, but the dispersed particles clustered back within a short time frame. Sample preparation prior to AFM and transmission electron microscopy (TEM) imaging appears to disperse clusters, but the clusters become visible in AFM when they are stabilized by Abs in solution. The clustered form of the virus appears to restrict access of Abs, lectins, and glycosidases to surfaces within the cluster. Mannosidase treatment following virus dispersion by filtration prevented clustering, suggesting that the mannose glycan shield is involved in the cluster formation. Free mucin molecules (porcine gastric mucin) effectively dispersed HIV-1 clusters, even those stabilized by Abs. HIV-1 loaded mucin dried on the AFM surface with a fern-like fractal pattern, similar to that seen clinically in cervical mucin during the more penetrable ovulation stage.

Importance:

The phenomenon of reversible clustering is expected to further nuance HIV immune stealth because virus surfaces can escape interaction with Abs by hiding temporarily within clusters. It is well known that mucin reduces HIV virulence, and current perspective is that mucin aggregates HIV-1 to reduce infections. Our findings however suggest that mucin is dispersing HIV clusters. The study proposes a new paradigm for how HIV-1 may broadly evade Ab recognition with reversible clustering and why mucin effectively neutralizes HIV-1.

Introduction:

The quest for HIV-1 treatment and cure started around 1983 when the virus was first isolated (1). With forty years of intense research, a vaccine for this virus still remains elusive (2). The purpose of a vaccine is to induce broadly neutralizing antibodies (Abs) that recognize and eliminate HIV-1 in circulation, but the virus has evaded such detection (3). Nevertheless, there have been significant advances in the treatment of HIV-1 with anti-retroviral drugs that target HIV-1 proteins and inhibit viral replication and maturation (4). Combined antiretroviral therapy (cART), targeting HIV-1 reverse transcriptase, integrase and protease, has enabled viral loads to be kept below the detection limit and allowed HIV patients to lead normal lives. However, this treatment does not eliminate the virus within patients (5). The virus remains latent in reservoirs within T cells and macrophages, ready to reactivate when there is a lapse in treatment (6). Eliminating the virus within a patient is further complicated by the virus's ability to mutate rapidly and tolerate a wide range of mutations (7). Drug treatment of HIV creates selective pressure for the emergence of escape variants of the virus which are more resistant to the treatment (8). Due to these complexities in treating HIV-1 infection, there is still an urgent need for a vaccine that can facilitate the production of broad neutralizing Abs against HIV-1 (6). Broad neutralizing Abs bind to conserved epitopes and receptor-interaction sites on the gp120 region of the envelop protein (Env), making the virus unavailable for infecting cells and thereby 'neutralizing' its virulence.(9, 10) A combination of features that are unique to HIV has made it difficult to develop a vaccine using neutralizing Abs (11). The virus mutates rapidly into divergent strains, and it has not been feasible to generate catch-all Abs that recognize the wide range of strain variation. Regions on the HIV-1 envelop protein that are accessible to Abs are also highly mutable and not essential for host interaction, while the more conserved and critical regions are protected by high-mannose glycans and thus inaccessible to Abs (12). The glycan coverage on HIV is substantial; the sugars make up almost half the weight of the virus (13). Additionally, the glycan attachment sites on the envelop proteins can also change constantly, adding another layer of variation to elude Abs (14). The ability of HIV-1 to disguise its surface with highly mutable epitopes and a shifting foliage of high mannose glycans has impeded the development of an effective HIV vaccine.

Arrays of mannose sugars were found to self-adhere with short-range brittle forces (15, 16). HIV-1 particles pseudo-typed with envelope proteins from Vesicular Stomatitis Virus (VSV) also adhered to each other in a Velcro-like manner when mannose residues in the glycan core were exposed and brought in contact with force spectroscopy (17). VSV-G HIV-1 also self-aggregated in solution when the mannose core was exposed (17). It is not known whether wild type HIV-1, with native gp120 Env rich with terminal high-mannose glycans, will also self-adhere and aggregate in solution. Several viruses, including VSV and polio, exhibit aggregate forms that are known to evade neutralizing antibodies (18, 19). The goal of the study is to determine if the mannose shield that confounds Ab neutralization of HIV-1 also induces the virus to aggregate, which may further nuance the immune stealth of HIV.

The solution behavior of HIV-1 in culture media containing serum proteins (i.e., virus media) was tracked with Dynamic Light Scattering (DLS), and the interpretations were corroborated with atomic force microscopy (AFM). While serum proteins in virus media contributed significantly to the DLS and AFM data, they did not interfere with

the virus behavior in solution and could be factored out in the observations with lectins, antibodies and mucin. When the serum contribution was excluded, almost all viral particles in solution appeared to be present in clusters of 400 – 700 nm hydrodynamic diameter (D_H). The lectins, Abs and glycosidases used in the study did not dismantle the clusters and had restricted access to the virus surfaces within the cluster. The HIV-1 clusters could be reversibly dispersed by filtration shear to pass through 0.2 μm filter pores as single particles, but which re-clustered back in the filtrate. However, mannosidase treatment of the dispersed virus in the filtrate prevented re-clustering. Antibody interaction with the dispersed virus also prevented re-clustering. Free mucin molecules effectively dispersed the viral clusters in solution, even those stabilized by Abs. The initial analysis was performed with replication-deficient HIV-1 that was pseudotyped with gp120 Env and produced in HEK 293T cells. However, the virus aggregation behavior was also evident in replication-competent HIV-1 produced in macrophages and T cells. Our biophysical study on the solution behavior of HIV-1 adds a new perspective to the broader questions of HIV-1 immune stealth and for the effectiveness of mucin in reducing HIV-1 infectivity.

Materials and Methods

Materials: HEK 293T cells for virus production were purchased from ATCC (Manassas, VA). HIV-1 proviral DNA, pNL4-3.Luc.R-E (HIV-Luc-G) containing two nonsense frame shift in the *Env* and *Vpr* genes with Luciferase reporter gene cloned in place of *Nef* was obtained from NIH AIDS Reagent Program (Germantown, MD). VSVG-expressing plasmid, pHEF VSVg, was obtained from NIH AIDS Reagent Program (Germantown, MD). HIV-1 Env expression vector (pLET-LAI) was a gift from Dr. Alberto Bosque (George Washington University). Antibodies to gp120 and VSV-G envelope proteins were obtained from Abcam (ab21179, Waltham, MA, USA) and Thermo Fisher Scientific Inc, (A00199-40, Piscataway, NJ, USA), respectively. Dulbecco's Minimum Essential Media (DMEM) and serum were obtained from Thermo Fisher Scientific Inc, (Piscataway, NJ, USA). Lectins used in the study and respective substrate sugars are listed in Table 1. All lectins were obtained from Millipore Sigma Inc. (St. Louis, MO) except for MAA and LEL (GlycoMatrix, Dublin, Ohio, USA). Lectins were diluted in 4 mM Phosphate Buffer Saline (Caisson Lab, Smithfield, Utah) to 1 mg/ml concentration. The solutions were supplemented with either 1mM $CaCl_2$ or 1mM $CaCl_2$/$MnCl_2$ ions (GlycoMatrix, Dublin, Ohio, USA) as recommended by the manufacturer. For many lectins, like ConA, the Ca ions that come with DMEM present in virus media were sufficient for activation. β-Mannosidase from *Canavalia ensiformis* (18mU/μL) was obtained from Sigma-Aldrich, Co., St. Louis, MO. Porcine Gastric Mucin- type II (PGM-II) from (M2378, Millipore Sigma Inc., St. Louis, MO) was dissolved in PBS pH ~7.35 to a stock concentration of ~4.5 mg/ml, filtered with 0.2 μm syringe filter (PES, Corning, NY). The 0.45 μm syringe filter (SFCA) was obtained from Corning, NY. T-tropic HIV-1(IIIB) and M-tropic HIV-1 BAL viruses were purchased from Advanced Biotechnologies (Eldersburg, MD).

Table 1: List of lectins used to detect terminal sugars and source

Lectin	Source	Catalogue number	Terminal sugar	Substrate linkage
ECA	*Erythrina cristagalli*	L5390	galactose	β-gal (1-4) GlcNAc
WGA	*Triticum vulgaris*	L9640	N-acetyl glucosamine	$(GlcNAc)_2$, NeuNAc
ConA	*Canavalia ensiformis*	L7647	mannose	α-man, α-glc
MAA	*Maackia amurensis*	2151007-1	sialic Acid	Sialic acid (α2 – 3)
LEL	*Lycopersicon esculentum*	21510074-1	N-acetyl glucosamine	β -(1-4) GlcNAc
SNA	*Sambucus nigra*	L32479	sialic Acid	Sialic acid (α2 – 6)

Virus preparation and 'virus media': HIV-1 Env pseudo typed viruses were generated by co-transfecting HEK 293T cells with HIV-Luc-G and gp160 Env expressing plasmids using Calcium-phosphate as previously described.(20) At 48 hours post virutransfection, supernatant containing viral particles and culture media was collected, cleared at 3,000Xg for 15 min and stored at -80°C until further use. The culture media containing virus was then transferred in 200µl aliquots to 4^0C and diluted with PBS at least 2 hours before use. The working pH of all diluted virus solutions and of control media was kept between 6.4 and 6.8 to avoid precipitation of supplemented Ca ions (typically at > 2mM) which increases with pH. The PBS-diluted virus preparation is referred to as 'virus media' to highlight the contribution of both serum proteins and virus in the DMEM solution to studies with AFM and DLS. The extent of dilution with PBS was determined by the need to get reliable DLS signal and keep the virus in dilute diffusion (where the correlation curves do not change with small changes in virus concentration). The latter is critical for tracking solution behavior with DLS because hydrodynamic diameters (D_H) are reliable indicators of size only for particles in dilute diffusion. Since the concentration of virus can change between different production stocks, the PBS dilution levels were adjusted for each stock to keep the intensity contribution from the virus and therefore the virus amounts approximately consistent. We note that because of variation in virus production efficiency in culture, the relative amounts of virus and serum in virus media and therefore the shape of its DLS correlation curves can vary between different production stocks. The control solution referred to as control media was fresh cell-culture media diluted in PBS to a similar extent. The response of control media was not significantly different than media without virus extracted from cultures of un-transfected HEK cells. To ensure that the solution effects observed in this study were intrinsic to the HIV-1 virus and not to its production from non-native HEK 293T cells, we also compared our findings with the virus media produced by HIV-1 infected macrophage and T-cells. The viral titer of the pseudotyped HIV, the T-tropic HIV-1(IIIB) and the M-tropic HIV-1(BaL) stock solutions was between 10^3 to 10^5 TCID50 (50% tissue culture infective dose). The stock solution was typically diluted between 5 and 20X with PBS.

Dynamic Light Scattering (DLS): The terminal sugars on virus, serum, and mucin were broadly profiled by tracking agglutination with different lectins in DLS. Agglutination or binding with lectins increases the size of diffusing species in solution, which appears as a rightward shift of the DLS correlation curves and an increase in corresponding species hydrodynamic diameter (D_H). Lectins were added to PBS-diluted virus/serum/mucin to obtain a final concentration of 0.1mg/ml. β-Mannosidase solution was added to PBS-diluted virus media to final working concentration of 1.8 U/μL. Antibodies were at 120 μg/ml (against VSV-G env) and 800 μg/ml (against gp120 env) final concentrations. All solutions were incubated for 1 hour at room temperature, and 50 μl was transferred to disposable DLS cuvettes (ZEN0040) for measurements. Malvern Zetasizer ZS (Malvern Instruments, Inc., Westborough, MA) with 632.8nm laser wavelength and 173º back-scatter angle was used for DLS. So that the correlation intensity between different samples can be compared, the optimal measurement parameters were determined and held constant for all samples: laser attenuation (~9), sampling position (4.65 mm), equilibration time (120 sec), and measurement time (150 sec). Rightward shifts of the DLS correlation curves indicate a decrease in the diffusion speed of the species. In dilute conditions, the diffusion speed of a species decreases because its size increases, which for viral particles can be caused by aggregation and binding. Similarly, leftward shifts indicate a decrease in the size of the diffusing species. Correlation curves show multiple exponential drops when diffusion species have significant size differences. The multiple exponential contributions were deconvolved with an in-house MATLAB software using the Sequential Extraction of Late Exponentials (SELE) algorithm.(21) The distribution of D_H in solution was obtained from the Zetasizer software (version 7). D_H is the size of a Stokesian bead having the same diffusion speed as the species in solution.

Atomic Force Microscopy: 1 μl of sample was adsorbed on a freshly cleaved mica for ~ 2 min under a weigh boat, washed with 100 μL distilled water (Chryster, Irvine, CA), and gently dried under Nitrogen stream. For imaging virus clusters, the virus media was pipetted gently without agitation. Samples were imaged with Bruker Multimode AFM having Nanoscope-V controller (Bruker Nanosurfaces, Inc., Santa Barbara, CA) in tapping mode with OtespaR3 cantilever (Bruker Nano Inc., Camarillo, CA). Images were flattened to compensate for non-planar scanner movement (Nanoscope Analysis 1.5, Bruker). NIH ImageJ software (https://imagej.nih.gov/nih-image/download.html) was used to obtain scatterplots of particle height and diameter by thresholding images, subtracting background height, and excluding particles of circularity <.25 to avoid artifactual diameters from closely-spaced particles that were not resolved as separate by the thresholding parameters. The area-diameter was calculated from the area of particles dried on imaging surface.

TEM imaging: 10μl of virus media was adsorbed to formvar, carbon-coated copper grid for 15 minutes. Excess sample was wicked away and the sample was fixed with 4% glutaraldehyde in 0.12 M Sodium cacodylate buffer for 5 minutes. The glutaraldehyde was removed with filter paper and the samples washed 4 times with water. The samples were then stained for 1 min with 1% aqueous Uranyl acetate. The grids were dried after wicking away the stain with filter paper. 80 KV in the FEI Talos F200X transmission electron microscope (Thermo Fisher Scientific, Hillsboro, OR) with Ceta 4M camera was used to image the samples

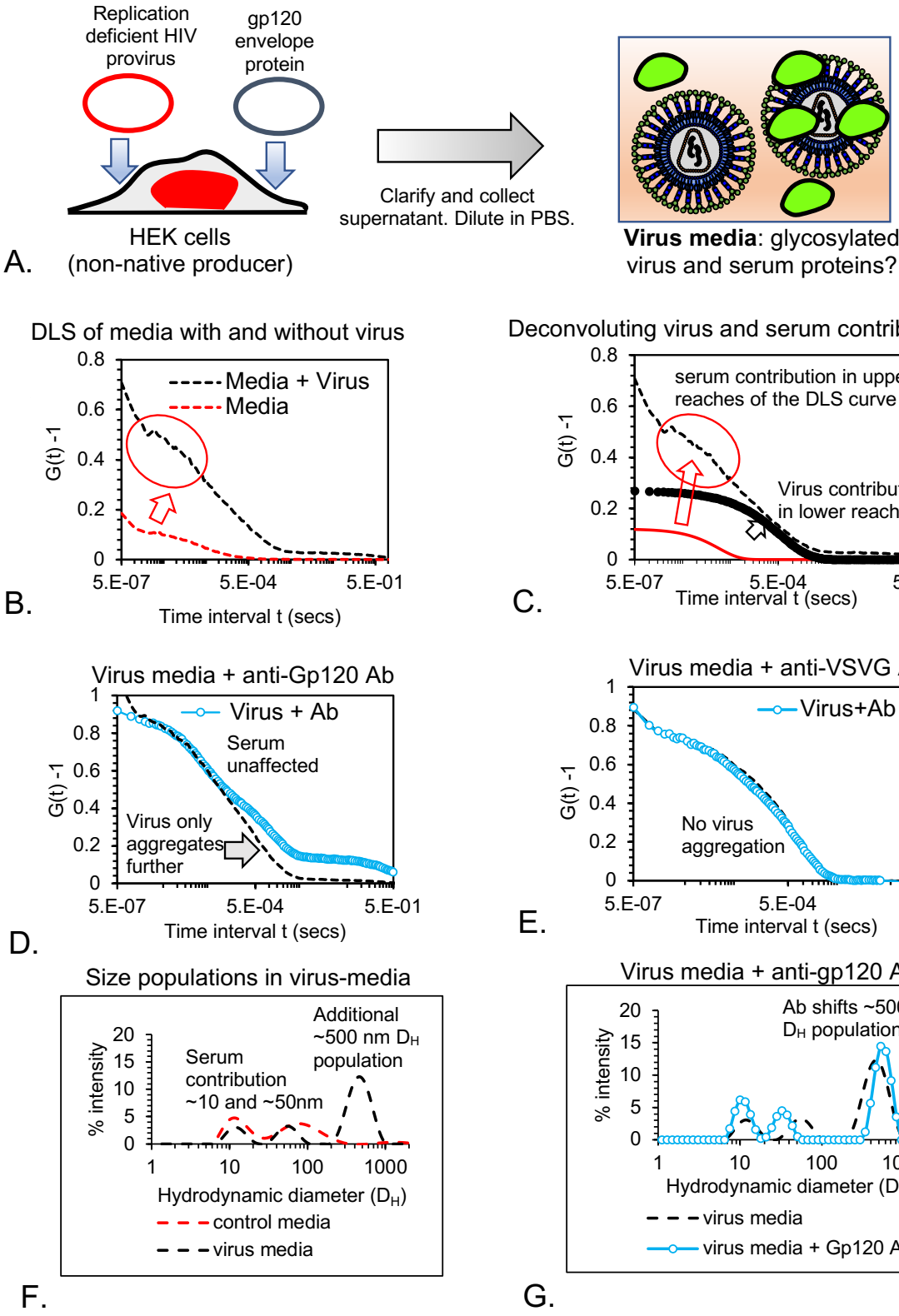

Figure 1: HIV-1 clusters in virus media: [A] 'Virus media' refers to clarified culture media from HEK 293T cells producing virus after transfection with plasmids for replication-deficient provirus and Gp120 envelop proteins. [B]

DLS correlation curves of virus media and control media (DMEM with FBS or serum proteins) showing significant contribution from serum proteins to both curves. Region of serum contribution to virus media DLS curve is circled. [C] Virus and serum contributions to the virus media DLS curve are relegated to the upper and lower regions of the curve. [D] Anti-gp120 Ab right-shifts or aggregates the lower region of the virus media DLS curve, confirming that HIV-1 particles are present in the larger diffusing species there. [E] Abs not specific to HIV-1 do not shift virus media DLS curve. [F] Histogram of the hydrodynamic diameters (D_H) showing the virus media has the ~10 and ~50nm peaks from serum proteins that are also present in control media. Additionally, a larger D_H peak appears in virus media likely from virus clusters diffusing in solution. [G] Anti-gp120 Abs increase the size of the larger D_H peak in virus media indicating that it is contributed by HIV-1 particles.

Results

3.1 Clustering of HIV-1 in culture media

HIV-1 Env pseudotyped virus was produced in HEK 293T cells as illustrated in Fig. 1A. The supernatant from cultured cells was clarified by centrifugation and diluted with PBS, referred to as 'virus media' to emphasize the presence of both virus and serum proteins in the preparation. The DLS correlation curves of virus media and the control media (DMEM with fetal bovine serum) are shown in Fig. 1B. The control media itself has a pronounced DLS signal (red line, Fig. 1B) due to the presence of serum proteins, which needs to be factored out to understand contribution of virus particles to virus media signal. In DLS, each population of particles with similar hydrodynamic diameter (D_H) or diffusion speed contributes a negative exponential to the correlation curve. For each negative exponential, the correlation intensity (y-axis) falls around the timescale (x-axis) over which the particles diffuse. Consequently, when the diffusion of the population slows down (i.e., as D_H increases), its correlation fall occurs at later time, seen as a rightward shift of the population's negative exponential (22, 23). A deconvolution of the virus media DLS curve shows that it is composed of at least two negative-exponential curves whose falls are well separated (Fig. 1C). One negative exponential contributes to the upper region of the virus media curve (circled in red, Fig. 1B), with its correlation fall at a time scale similar to control media, and it is therefore likely to be derived from the serum proteins diffusing in the virus media. A second negative exponential contributes to the lower region of the virus media curve (Fig1B, black curve), occurring only when virus is present in the media, and corresponds to a D_H in the range of ~500 nm.

Antibodies (Abs) against gp120 were added to virus media to confirm if the deconvolution of the DLS curves was accurate in capturing the presence of two diffusing populations, and to determine if viruses were present in the population contributing to the lower region of the curve. The anti-gp120 Abs right-shifted or aggregated only the lower region of the virus media DLS curve (Fig. 1D), suggesting that two distinct populations were contributing to different regions of the DLS curves. The lack of right-shift of the upper or serum region of the virus media DLS indicated that neither free virus nor free gp120 Env were present in the smaller diffusing population, and that the anti-gp120 Abs did not bind serum proteins. To ensure that the right-shifts in DLS were caused by Abs-induced aggregation or coating of virus and not by non-specific aggregation, a check with non-specific Abs was also performed (Fig. 1E). Polyclonal Abs against VSV-G, the envelop protein on Vesicular Stomatitis Virus, failed to shift the upper or lower region of the DLS curve from virus media (Fig. 1E). Collectively, these observations indicate that

the anti-gp120 Abs were specifically recognizing the 500 nm D_H species in the lower region of the virus media DLS curve, and that this species was covered with gp160 Env protein.

Figure 1F shows the distributions of hydrodynamic diameter (D_H) in the virus and control media as deconvoluted by the instrument software. Control media (i.e., DMEM supplemented with FBS) has populations with ~10 nm and ~50 nm D_H peaks, which are also observed in pure FBS solutions (Suppl. Fig. 1). While the first, smaller population is of the size expected for free protein, the D_H of the second larger population suggests that a fraction of serum proteins may be aggregated. Both these populations in control media were also present in virus media, along with a new ~500 nm population appearing in the latter. Anti-gp120 Abs only shifted the ~500nm population, confirming that the virus was present in it (Fig. 1G). Since HIV-1 particle size in electron microscopy ranges from 90 nm to 160 nm (24), the 500 nm population in virus media is likely aggregates or clusters of viral particles. The appearance of these clusters was not influenced by the extent of supplementation with serum (Suppl. Fig. 1B), by the extent of dilution with PBS (Suppl. Fig. 2), or by the type of producer cells (Suppl. Fig. 3). Media containing replication-competent HIV-1 from macrophages and T cells also demonstrated >200 nm D_H peaks (Suppl. Fig. 3). “Bald” HIV-1 virus produced without gp160 Env did not form clusters, indicating that the clustering was likely mediated by the viral envelope protein and not the envelope membrane (Suppl. Fig. 4). Abs against gp120 did not right shift virus media containing “bald” viruses as well (Suppl. Fig. 4).

3.2 Viral clusters in solution are reversibly aggregating

Particles from control media and virus media were analyzed with AFM imaging. AFM phase images (top) and corresponding height images with color map spanning 13 nm span (bottom) are shown (Figs. 2A-C). The AFM phase images highlight the changing interactions at the AFM probe as the latter scans the imaging surface. The phase image for control media had a rich presence of serum proteins (Fig. 2A, above). Since majority of the serum proteins had height less than 6 nm, they were not visible in the corresponding height image for the chosen colormap (Fig. 2A, below). For virus media, the phase image showed two types of particles additionally (Fig. 2B, above), which could be distinguished more clearly in the height image whose colormap excluded serum contribution (Fig. 2B, below). One type of these particles had a diameter of ~80nm diameter, with a height > 10nm (highlighted with star), and thus appeared saturated in height color map of Fig. 2B. The other population was in the 30-50 nm range and had a height of < 10nm (Fig. 2B, highlighted with red arrow). A zoomed-in image (Fig. 2C) showed that the ~40 nm particles were breaking off from the ~80 nm particles (see arrow in Fig. 2C). Negatively stained TEM images of the virus media also showed both types of particles, confirming that these were not AFM imaging artifacts (Fig. 2E). The TEM negative staining showed spikes on both populations (Fig. 2F), as well as cones of both sizes on the sampling surface and inside the viruses where the stain had penetrated (Fig. 2E). Associations between ~40 nm particles like those seen in AFM images were also observed in TEM (Fig. 2F). The TEM and AFM images confirmed that ~80 nm viral particles, within the size range expected for HIV-1, are present in the virus media. It is not clear whether the ~40 nm particles were sections broken off from larger viruses or were smaller viruses themselves.

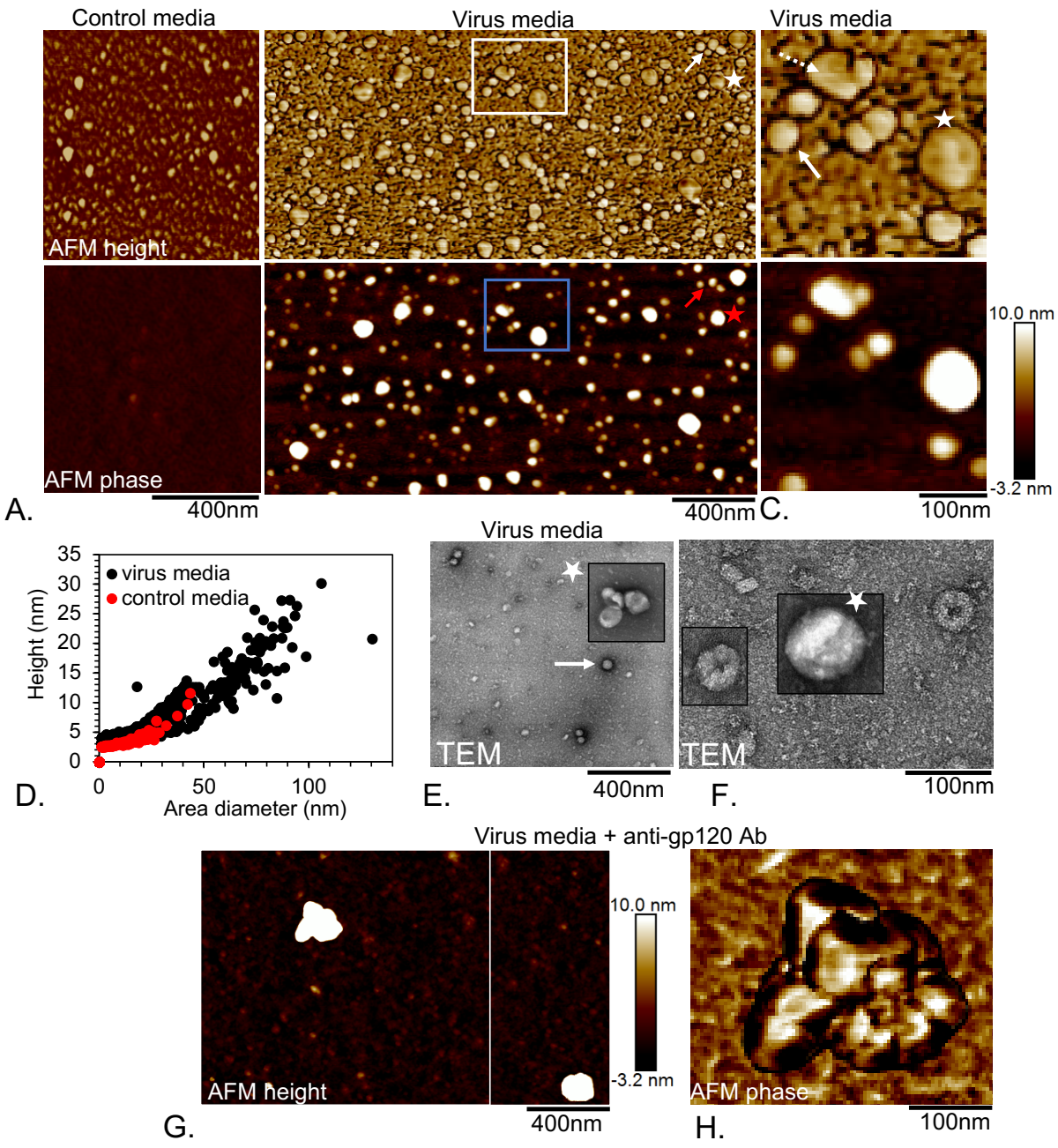

Figure 2: Imaging of particles in HIV-1 virus media: [A] AFM of control media shows serum proteins in the phase image (top), but which are not apparent in corresponding height image (bottom) having color bar spanning 13 nm. [B] AFM of virus media showing serum and virus in phase image (top) but with the non-serum particles alone highlighted in the color map of the height image (bottom). There are ~40 nm (arrow) and ~80 nm (stars) particles appearing in virus-media. [C] Zoomed-in phase (top) and height (bottom) image highlighting the ~80nm (star) and ~40nm (arrow) particles appearing in virus media. In one instance, the ~40nm particle appears to be breaking off the 80nm particles (broken arrow). [D] Particle analysis of multiple AFM images showing serum particles with similar height vs. diameter trend in both control and virus media, and that virus media has new contributions from particles >40 nm with different height vs. diameter trends (n = 3 samples). [E] Negatively-stained TEM of virus media showing both ~80nm (star) and ~40nm (arrow) particles. [F] Envelope spikes are seen on ~80nm particles and free viral cones are visible inside and outside the ~50nm particles suggesting that these are both viruses. [G,H]

Supplementing virus media with anti-gp120 Abs stabilizes the HIV-1 clusters in solution for being visible in AFM imaging. Larger clusters of ~80nm viral particles are observed in virus media with anti-gp120 Abs.

Figure 2D presents a scatterplot of particle heights vs. area-diameter summarizing the populations observed in AFM images. It also serves to compare against the population histogram observed in DLS (Fig. 1F). AFM particle analysis showed that serum in control media had particles ranging from the diameter of single to clustered proteins (Fig. 2D, red points), which is consistent with the two serum D_H populations being observed in DLS (Fig. 1E). The signature height vs. diameter trend of serum particles observed in control media was also present in virus media (Fig. 2D), again being consistent with similar serum D_H peaks being observed in DLS for both control and virus media. However, additional particles with area-diameters 40 – 100 nm and a height vs. diameter trend different than that of serum were observed in AFM imaging of virus media (Fig. 2D). In contrast, particles that were observed in DLS had 500 nm D_H. There were no clustered particles observed in AFM and no distinct increase in ~80 nm D_H population in DLS, suggesting that the virus clusters in solution were prone to breaking into single virus particles during sample preparation for imaging. On the other hand, when virus media was supplemented with anti-gp120 Abs, large (>200 nm) clusters of ~80nm viral particles become evident in AFM imaging (Fig. 2G, H). There was a noticeable increase in the AFM heights of these imaged clusters, and the 3D nature of the viral associations validated that the virus clustering was not surface induced. Thus, it appears that while HIV-1 clusters in solution are prone to being dispersed on surface, while Abs stabilize the solution clusters enough for them to remain undispersed on AFM surfaces.

To understand the dispersal characteristics of the HIV-1 clusters, virus media was filtered through membranes with 0.2 μm pore size. As summarized by the DLS histogram taken 15 min after filtration, the filtrate lost the ~500 nm D_H population and instead had a ~190 nm D_H population (Fig. 3A). Over 1 hr time, however, the ~500 nm D_H population reappeared (Fig. 3A). The DLS correlation curves in Fig. 3B showed near recovery of virus clustering 1 hr after filtration (see scaled data in Suppl. Fig.5). The scattering intensity of the recovered clusters was within 10% of that in unfiltered virus media (Fig. 3B), indicating that majority of the viral clusters in virus media passed through the smaller filter pores as dispersed particles or as partial clusters. That is, viral clusters were not being retained on the filter membrane which would have led to a significant decrease in the scattering intensity of the filtrate. In other words, the clustered state was the thermodynamically stable state for HIV-1, but the clusters could be easily dispersed by filtration shear, and possibly during sample preparation in AFM or TEM imaging. The reversible clustering of HIV-1 interpreted from the filtration experiment is schematized in Fig. 3C. To corroborate the interpretation that filtration was dispersing virus clusters, virus media was imaged in AFM without imparting any shear forces of mixing during sample preparation. Several larger clusters of ~80 nm viral particles became visible on the surface (Fig. 3D). Under the same conditions, only single virus particles were evident in AFM images of virus media taken immediately after filtration (Fig. 3E). To confirm further that virus was being dispersed by filtration, virus media was filtered into a solution of anti-gp120 Abs. The filtered viruses did not cluster back in this case (Fig. 3F) and AFM images of the solution showed dispersed HIV-1 virus surrounded by Abs (Fig. 3G). The absence of re-

clustering in Abs-bound dispersed virus also indicated that the clustering impetus was coming from the gp120 Env of HIV-1.

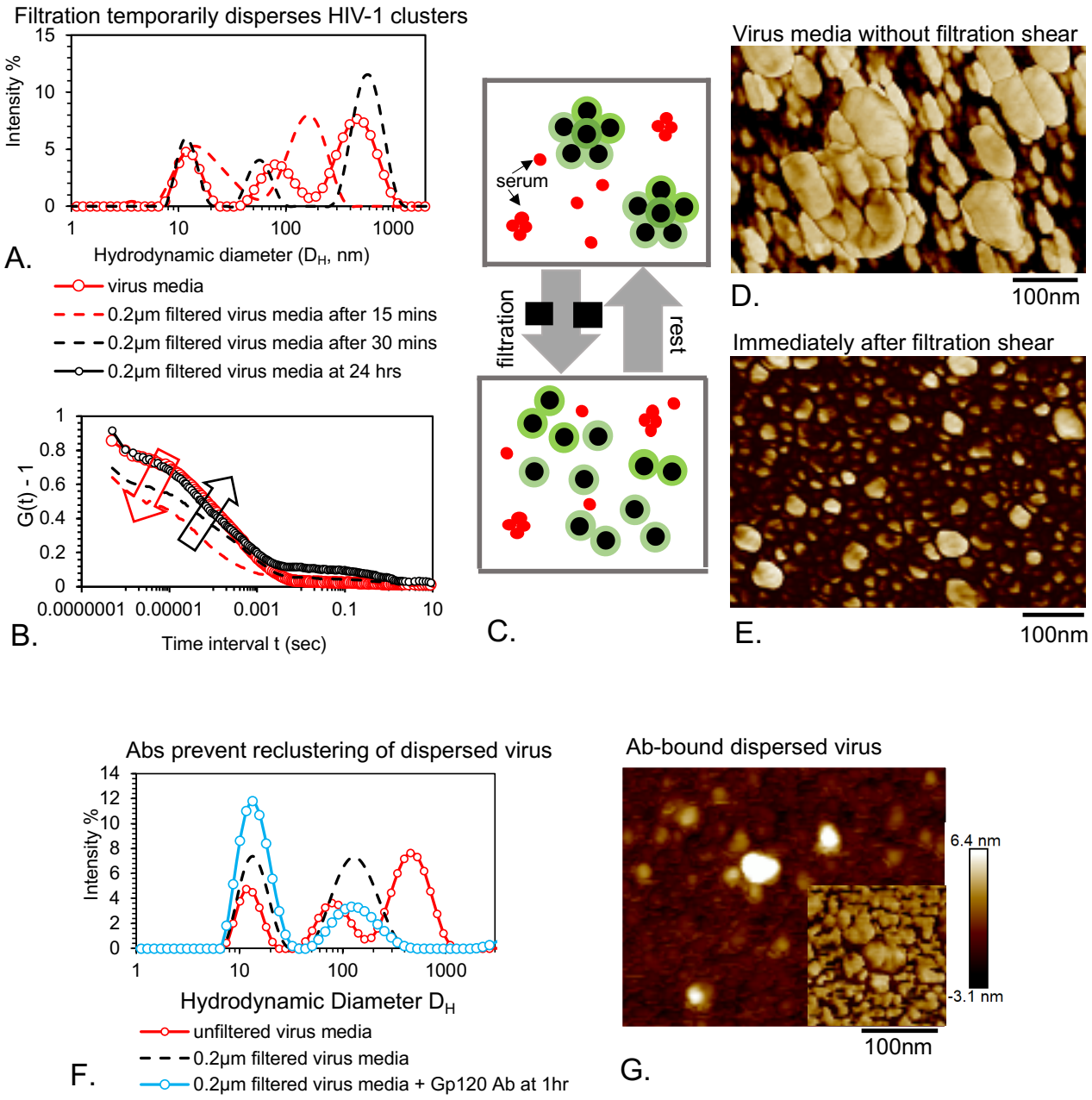

Figure 3: HIV-1 clusters are reversibly dispersed by filtration: [A] Distribution of population sizes, D_H, in virus media before, immediately after, and after filtration. The ~500 nm virus clusters reduce to ~190 nm size in the filtrate immediately after filtration, but over time the clustering recovering. [B] DLS correlation curves showing reduction in the size of viral contribution immediately after filtration (left-shift in immediate-time filtrate) and the re-clustering of the virus over time (DLS curves of long-time filtrate and unfiltered overlap). [C] Schematic highlighting the reversible dispersal and recovery of HIV-1 clusters implied by the filtration experiment. [D] AFM phase image of undisturbed virus media before filtration showing HIV-1 clusters. [E] AFM phase image of undisturbed virus media immediately after filtration showing dispersed HIV-1 particles. [F] DLS histogram showing that HIV-1 clusters which are dispersed

by filtration into anti-gp120 Ab solution do not re-cluster back. [G] AFM height and phase image of virus dispersed into antibody solution showing dispersed virus covered by Ab like particles.

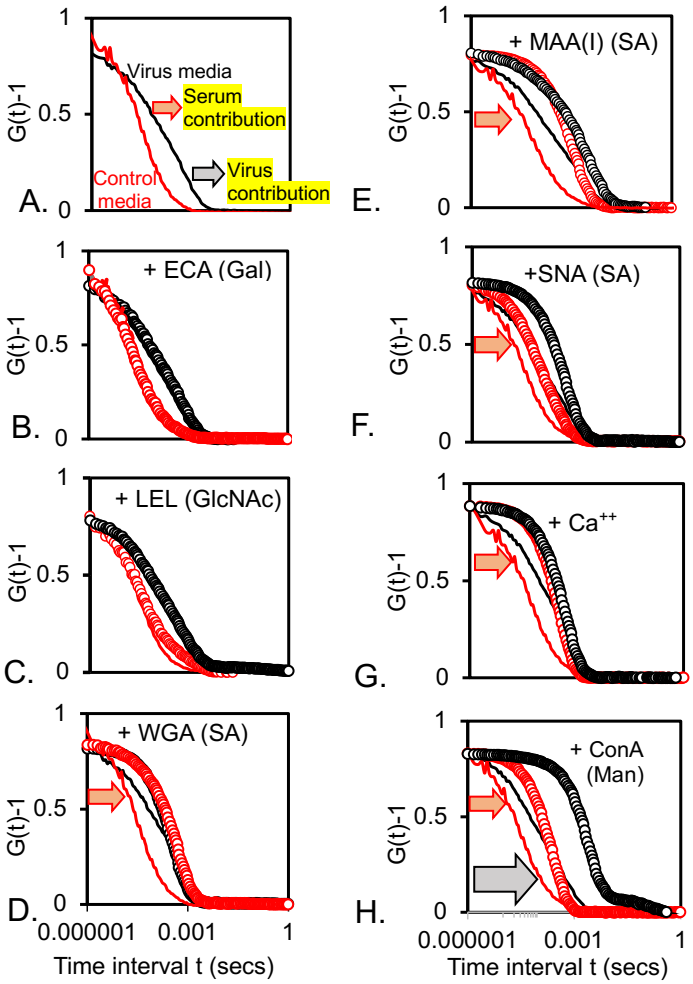

Figure 4: Glyco-profiling of terminal sugars on serum and HIV-1 populations in virus-media: [A] Scaled DLS curves of control and virus-media, highlighting that serum and virus contribute to different regions of the virus-media curve. Lectins ECA [B] and LEL [C] did not shift the virus media and control media curve, indicating that terminal galactose and glcNAc are not predominantly present on both populations. Lectins WGA [C], MAA [D], SNA [E], and Ca [F] shifted the control media and the upper regions of the virus-media alone, indicating that terminal SA is present on serum but not on virus. Lectin Con A [G] shifted virus-media extensively and serum to some extent indicating it is extensively present on the virus contributing to the lower region of the virus-media curve.

3.3 Viral clusters are covered with mannose glycans and mannosidase treatment interferes with clustering: Since the virus and serum population contribute to the lower and upper regions, respectively, of the virus media DLS curve, one can identify the predominant terminal sugar on each population from which region of the curve shifts upon lectin addition. and by further confirmation using control media. Table 1 lists the lectins used in this study and the terminal glycan sugars they target. Figure 4 shows the DLS-based glyco-profile of virus media in conjunction with control media. Panel A displays the base curves without lectin addition. Lectins ECA (target: Galactose) and LEL (target: GlcNAc) did not shift virus media and control media DLS curves (Fig. 4B, C), indicating that galactose

and GlcNAc were not present as terminal glycan sugars on both serum and virus to extents sufficient for lectin agglutination. Lectins WGA (target: SA, GlcNAc-GlcNAc), MAA (target: SA), and SNA (target: SA ($\alpha 2-6$)) produced right-shifts in the control media curve and in the serum region of the virus media curve (Fig. 4D, E, F), indicating that the serum proteins but not virus clusters had terminal SA residues sufficient for agglutinating lectins. Calcium ions, which is typically added along with lectins like ConA, right-shifted or aggregated serum in control media but not in virus media (Fig. 4G). Lectin ConA (target: mannose) produced limited aggregation of serum but extensive right-ward shift or aggregation of the virus media curve indicating its predominant presence on virus (Fig. 4H).

AFM imaging was performed to validate the interpretation of the nature of DLS shifts as the aggregation of serum or virus by lectins (Suppl. Fig. 6). Aggregated serum particles were observed in AFM images when WGA or Ca was added to control media, but not when ECA or LEL was added, consistent with the former shifting the control media DLS curves but not the latter. Con A produced small aggregates with serum proteins and large aggregates with virus media. No large aggregates were observed when other lectins were added to virus media. These observations suggest that lectin-binding of serum and virus can be profiled independently using DLS and indicate that the HIV-1 clusters were covered with mannose glycans despite being produced in non-native HEK 293T cells.

To understand the role of mannose in HIV-1 clustering, virus media was incubated with β-mannosidase, a glycosidase that cleaves below terminal mannose and exposes GlcNAc residues. Following the incubation with β-mannosidase, the DLS curves of virus media shifted slightly leftwards in the lower region alone (Fig. 5A). DLS histograms confirmed that the size of HIV-1 clusters decreased from ~500 nm to ~250 nm (Fig. 5B). The mannosidase-cleaved virus media did not aggregate with ConA lectin (Fig. 5C), but instead aggregated with LEL (GlcNAc lectin) and WGA (GlcNAc-GlcNAc, SA), thereby confirming the loss of mannose residues and exposure of GlcNAc residues on the virus clusters (Fig. 5D, E). It appears that when mannosidase is added directly to HIV-1 clusters in virus media, it removed mannose from the surface of the clusters without eliminating but only reducing the size of the HIV-1 clusters. On the other hand, when mannosidase was added to HIV-1 dispersed by filtration, the diffusing size was reduced to that of single virus and re-clustering was prevented (Suppl. Fig. 7). It appears that while the removal of mannose sugars interferes with HIV-1 clustering, the clustering itself interferes with glycosidases accessing the HIV-1 surfaces within the cluster.

Interestingly, the DLS of the mannosidase-incubated virus media did not right-shift anymore with MAA lectin (target: SA) in the serum region. The loss of terminal SA from serum indicates that β-mannosidase likely cleaved as an endoglycosidase and exposed core GlcNAc residues on both virus particles with high-mannose glycans and serum particles with SA-terminated complex glycans. Correspondingly, AFM images of mannosidase-incubated virus media showed extensive retention of the ~80nm viral particles compared to regular virus media (Figs. 5F, G). The phase texture of these particles appeared different, and their heights were shorter compared to the uncleaved virus with the same height color map (Fig. 2). The mannose-cleaved virus appeared to adsorb non-randomly on the AFM surface, which could be indicative of their altered clustered state in solution (Fig. 5H) or a surface drying effect for

viruses now covered with hydrophobic GlcNAc sugars. While removal of mannose appears to have predominantly occurred on the cluster surface, it appears to change the texture of the virus adsorbed in AFM and reduce the size of solution clusters.

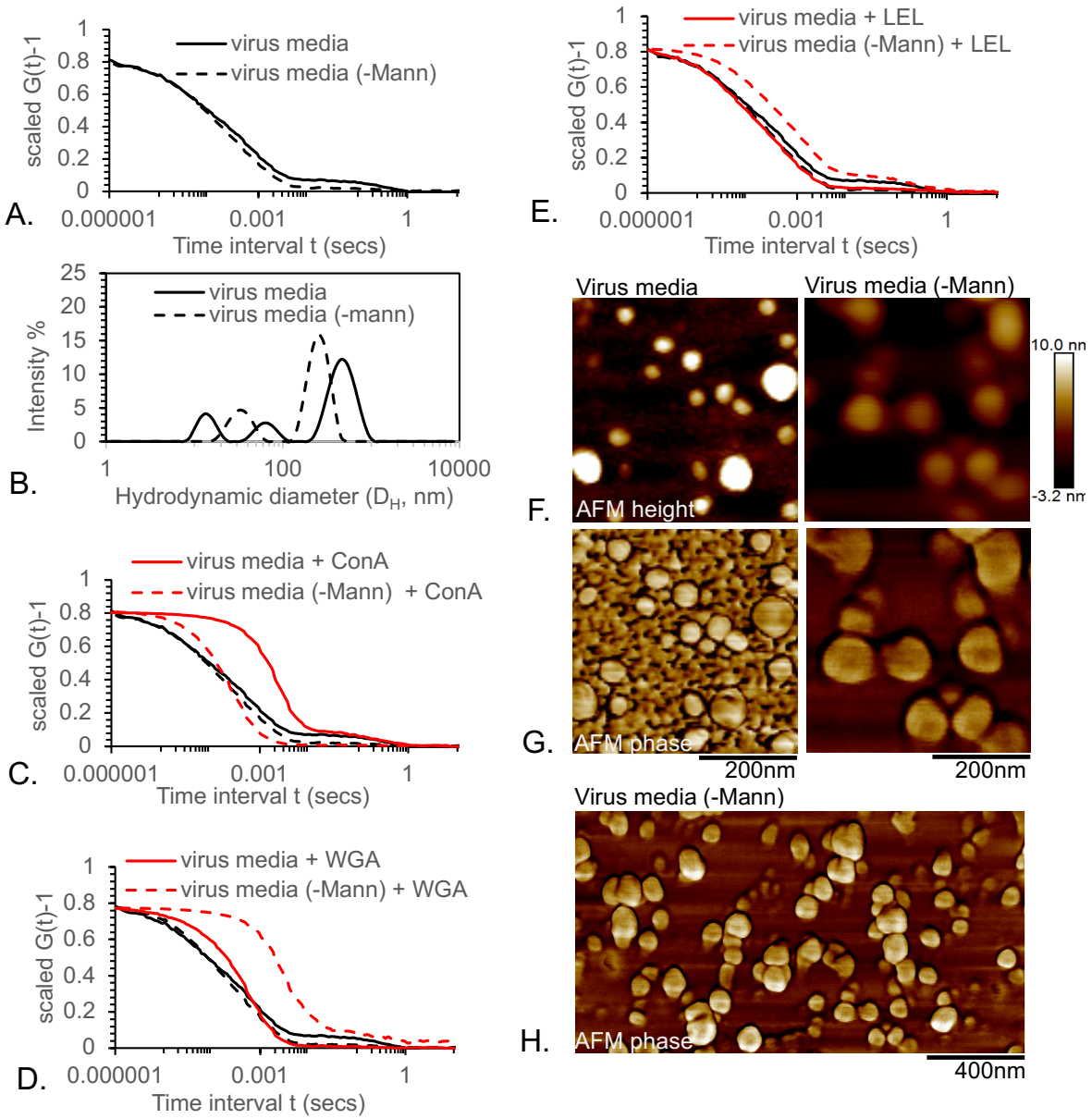

Figure 5: β-mannosidase treatment of virus media: [A] β-mannosidase cleavage left-shifts the lower region of the DLS curve contributed by virus-clusters. [B] DLS size histograms showing mannosidase treatment to decrease viral clusters from ~500 nm to ~ 200 nm D_H. [C] Mannose lectin Con A aggregates virus media (right-shift) but not mannosidase-cleaved virus media, confirming removal of mannose from cluster surface in the latter. [D] Mannosidase-cleaved virus, but not the uncleaved control virus, is aggregated by WGA confirming surface exposure of either SA or GlcNAc. [E] Mannose-cleaved virus alone is aggregated by GlcNAc lectin LEL, confirming the exposure of GlcNAc residues from glycan core following the mannose removal. [F] ~80 nm viral particles of lower height are visible in AFM images (right) following mannose removal and GlcNAc exposure. Uncleaved virus is shown for reference (left). [H] Non-random adsorption of mannose-cleaved virus on AFM mica surface

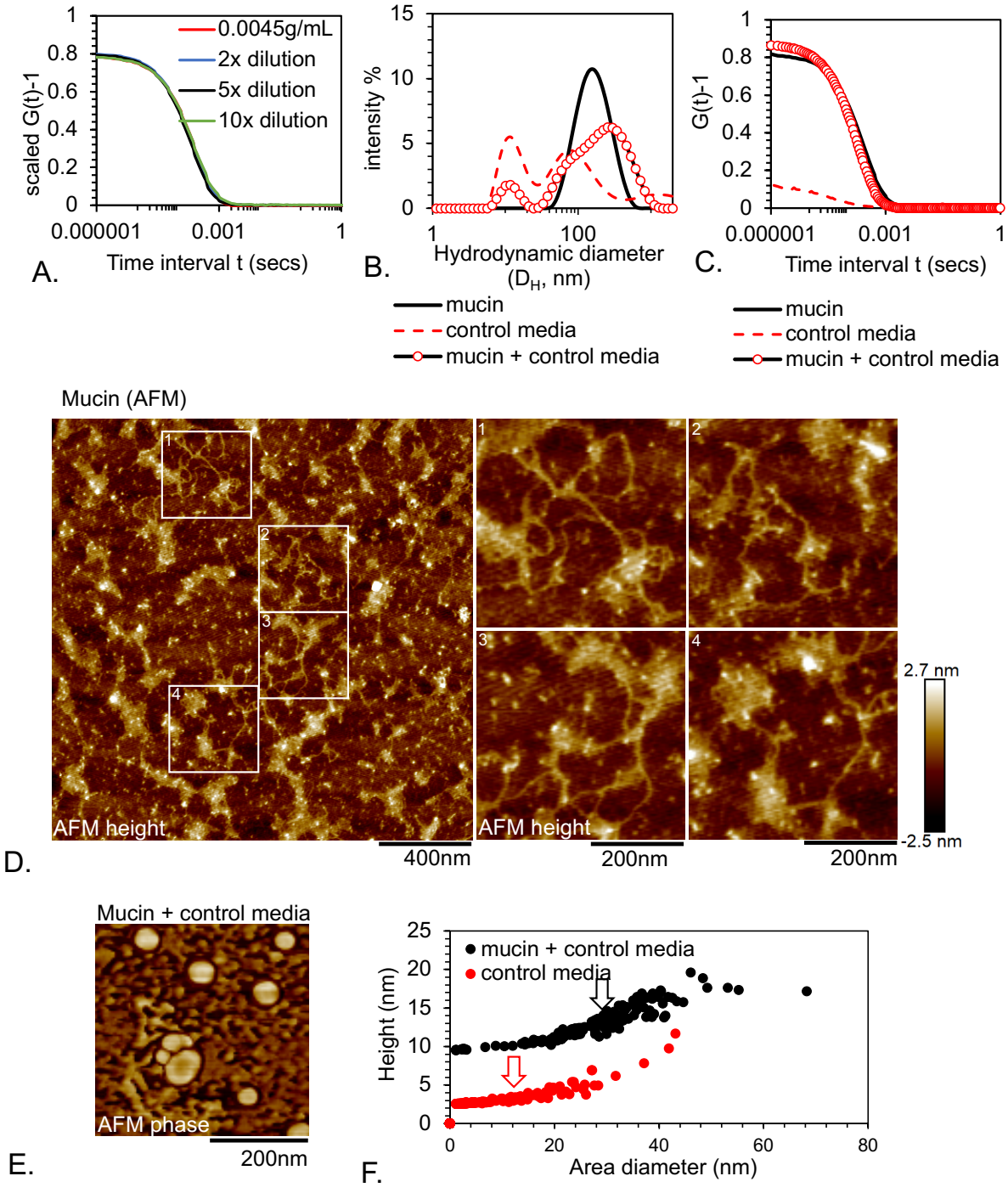

Figure 6: Characterization of baseline mucin and serum interactions: [A] Different dilutions of porcine gastric mucin solution in PBS showing that the diffusion speed of the mucin molecules does not change with dilution (i.e., curves do not shift) and therefore the mucin molecules are in free state without dominant inter-mucin interactions. [B] Histogram of hydrodynamic diameters (D_H) in solution showing that the solution of free mucin with control-media (i.e., serum proteins) has the same population D_H as control media and mucin alone. [C] DLS correlation curves showing that the mucin+control media curve is nearly the sum of the mucin and control-media curves, indicating that there is no major interaction with mucin and serum occurring that would change the type of diffusing species. [D] AFM Images of mucin molecules forming networks in AFM surface shown at two different scales. [E] AFM phase image of serum+mucin highlighting distinguishable serum particles present amidst the adsorbed mucin. [F] Particle

analysis of serum+mucin AFM images showing that while serum particles in mucin have similar height vs. diameter trends to serum alone, there is a higher sampling of aggregated serum particles when in the presence of mucin. Arrow marks the 50th percentile particle. The higher heights of mucin+serum particles reflect the mucin layer adsorbed below the serum particles.

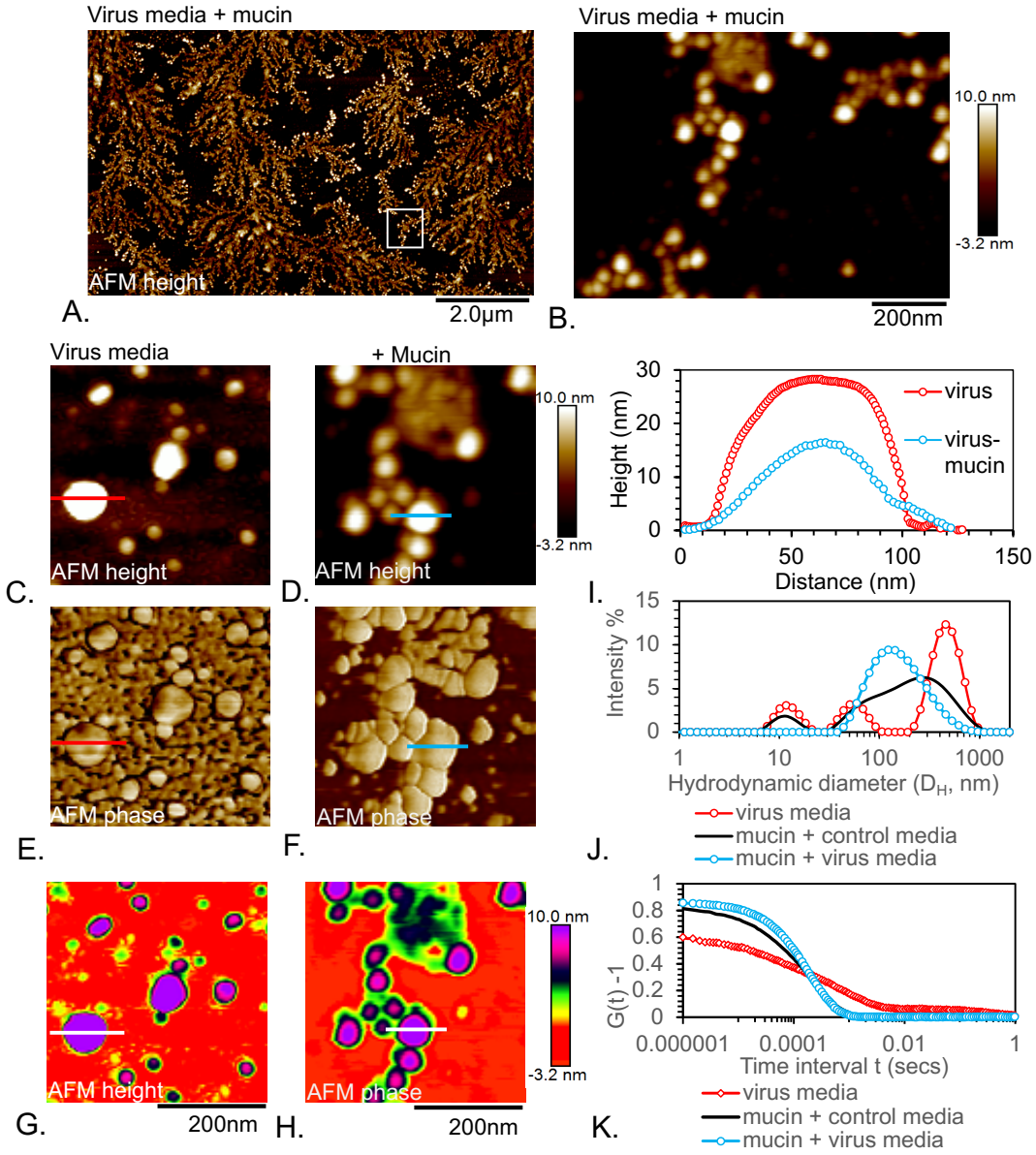

Figure 7: Mucin disperses HIV-1 clusters: [A] Mucin loaded with virus adsorbs in fern fractal form. [B] Zoomed in image of mucin arborization in the presence of HIV-1. [C-H] AFM height, phase, and height with multicolor map of virus (left) and of virus coated and trapped in mucin. [I] Height profile comparing virus in media and in mucin. [J] DLS histogram showing that the multiple diffusing populations in virus-media and in mucin with control media are replaced by a single diffusing species around ~120 nm D_H in the mixture of virus media and mucin. Notably the ~700 nm D_H from virus clusters in virus media is lost. [K] DLS Correlation curve showing the loss of HIV-1 clusters (left shift of virus curve) when mucin is added.

3.4 Mucin disassembles HIV-1 clusters into virus mucin interaction units: The goal was to understand how free mucin molecules affect virus clusters. In the absence of inter-mucin interaction, any change in the D_H of diffusing species in control- or virus- media when mucin is added would reflect mucin interactions with these species. Also the baseline interactions between mucin and serum were established before probing how mucin affected virus clusters in serum-media.

Porcine gastric mucin - type II (PGM-II) was diluted, filtered, and used in a concentration range where inter-mucin interactions did not have an effect, i.e., where the mucin D_H became independent of mucin concentration (Fig. 6A). The free mucin molecules displayed a D_H of ~100 nm (Fig. 6B). When control media was mixed with the free mucin molecules, the mixture showed all the D_H populations from the mucin and control media individually (Fig. 6B). Similarly, there was no significant alteration in the intensity and shape of the DLS correlation curves that would indicate the formation of a new diffusing species (Fig. 6C). These observations suggested that mucin and serum did not interact strongly to form a new diffusing species. Free mucin molecules formed network architecture when dried on AFM surface (Fig. 6D). This network architecture reflects mucin structure, which consists of an extended regions with O-glycans, separated by globular domains that interact with each other. When serum was added to mucin, AFM images displayed distinguishable serum particles overlaid on the mucin background (Fig. 6E). Image analysis of the serum particles revealed that they had the same height vs. diameter trend as control media (Fig. 6F). The recorded heights of serum proteins were higher, however, when present with mucin, possibly because of mucin coating the background. Arrows indicate the 50^{th} percentile particle in the height vs. diameter distribution of serum proteins in control media and in mucin (Fig. 6F). This suggests that there is an increased occurrence of larger serum particles in the presence of mucin than without (Fig. 6F). While it can be argued that particle distributions mapped with AFM imaging may have sampling artifacts, the DLS histogram also corroborates a similar change in distribution with the smaller serum peak diminishing compared to the larger serum peak when mucin is present (see Fig. 6B). These changes in serum distribution suggest that free mucin molecules may be favoring the aggregated state of serum proteins.

When virus media is mixed with free mucin molecules, adsorbed on a mica surface, and imaged by AFM, the networked architecture of mucin observed in AFM (Fig. 6D) changed into a ‘fern’ fractal or arborized architecture (Fig. 7.A, B). These fern branches were comprised of dispersed units about the size of single HIV-1 particles, within mucin entrails (Fig. 7B). The make-up of the fern branch becomes apparent when three representations of an imaged region were considered in conjunction and compared against virus media alone (Figs. 7C-H). Figure 7I shows the height section across a virus (Fig. 7C) and a dispersed unit in a mucin+virus fern (Fig. 7D). While the diameters were comparable, the height of the mucin+virus unit is much reduced. It is not clear if the reduced height results from changes in the sample-probe interactions or from changes in the nature of sample drying or in the sample itself. The corresponding AFM phase image (Fig. 7F) shows similar surface texture for both the virus and mucin regions within the image (unlike that observed for mucin and serum in Fig. 6E), suggesting that the virus may be covered with mucin. A multi-color map highlighting both the lower and higher ends of the height spectrum further

corroborated that the regions of uniform phase interaction in Fig. 7F had distinctly higher regions of single virus (purple, red) trapped within lower regions of mucin (green, black**)** (Fig. 7H). Taken together, the AFM images suggest that HIV-1 alters the inter-mucin interactions exhibited when mucin alone dries on AFM surface, and that the virus gets covered by mucin. Concurrently, DLS histogram showed that the landscape of diffusing populations changed when virus media was added to mucin solution (Fig. 7J), unlike when control media was added to mucin (Fig.6B). The large D_H corresponding to virus clusters in media disappeared, and instead a single population around 120 nm D_H appeared (Fig. 7J). This suggests that free mucin molecules disperse the large clusters of HIV-1. It does not seem likely that the ~120 nm D_H population consists of separately diffusing free virus and free mucin units, as there would be a marked increase in the scattering intensity in that diffusing region to reflect the addition of separate virus and mucin scattering volumes (Fig. 7K). Since there was no significant increase in the intensity of the correlation curves for the mixture (Fig. 7K), it is possible that ~120 nm D_H diffusing species are units of interacting virus and mucin, which is consistent with the AFM observation that the virus is covered by mucin.

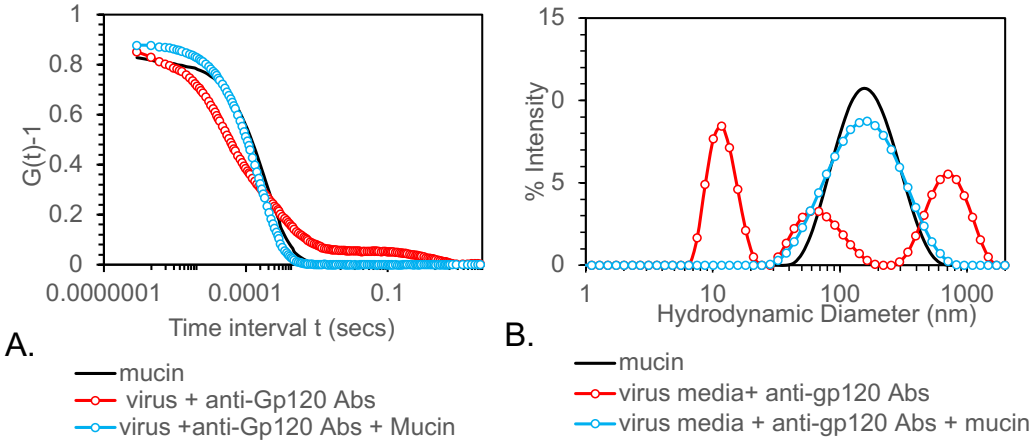

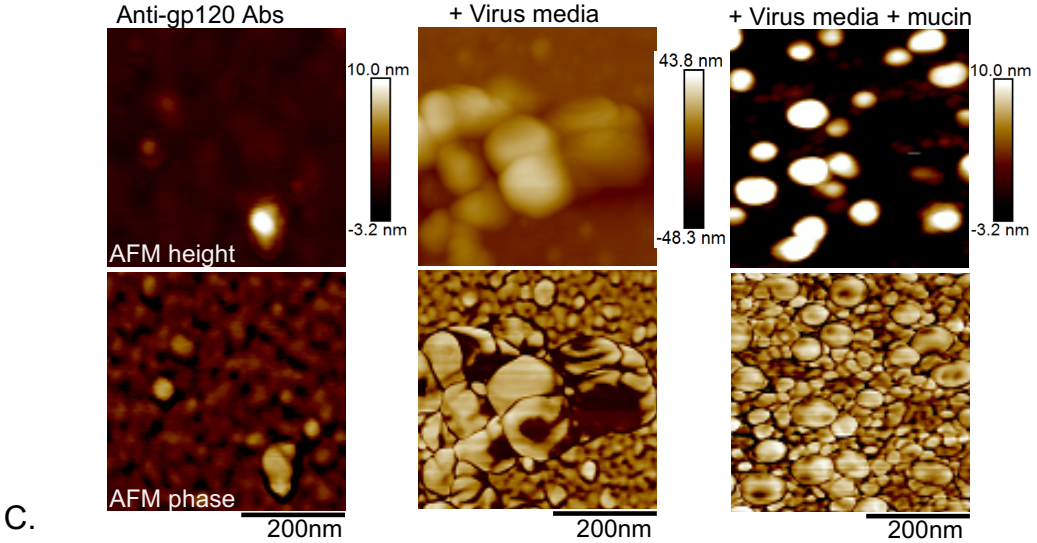

Figure 8: Mucin disperses HIV-1 clusters stabilized by antibodies: [A] DLS Correlation curve showing that mucin disperses (left-shifts) virus clusters stabilized by anti-gp120 Abs. [B] DLS histogram showing the loss of the > 500 nm D_H virus clusters stabilized by anti-gp120 Abs peak when mucin is added. [C] AFM height (top) and phase (bottom) images showing anti-gp120 Abs (left), viral clusters stabilized by anti-Gp120 Abs (middle), and loss of viral clusters when mucin is added to the mix (right).

The strength of mucin dispersal of HIV-1 clusters was examined by mixing mucin with virus media stabilized by anti-gp120 antibodies (Fig. 8). DLS correlation and histogram curves again showed dispersion of the Ab-stabilized viral clusters (Fig. 8A, B). AFM imaging further confirmed that while anti-Gp120 antibodies (left panel in Fig. 8C) stabilized viral clusters for imaging (center panel in Fig. 8C). Upon mucin supplementation, only single viral particles and not viral clusters became visible (right, Fig. 8C).

DISCUSSION:

HIV-1 virus is covered by a shield of high-mannose N-glycans, which is known to impede antibody neutralization of the virus by obscuring viral surfaces critical for fusion and host entry. Recent studies showed that mannose-rich surfaces exhibit short-range Velcro-like adhesion to each other (15-17), The aim of the study was to determine whether such short-range mannose-mannose adhesions also applied to the high-mannose glycan shield of HIV-1, resulting in the virus aggregating in solution. We also examined how such clustering would affect HIV-1 interaction with entities such as antibodies, lectins, glycosidases, and mucin, which influence virus availability for infection. Figure 9 illustrates how these entities affect HIV-1 clustering based on the AFM and DLS observations.

Virus-media contains serum and reversible clusters of HIV-1: Cell culture media containing virus particles ('virus media') was found to have a significant amount of serum proteins, which had to be taken into account in DLS and AFM observations (Fig. 1A). These serum proteins came from the FBS added to the minimum essential media for culturing HEK 293T cells. Two populations of serum proteins were observed to be diffusing in both control media (without virus) and virus media: one had D_H of ~10 nm, which is in the size range for single proteins, and the other had D_H of ~50 nm, likely composed of small aggregates of serum proteins. The addition of virus into media introduced a new diffusing species having ~ 500 nm D_H. This size than the 90 – 120 nm range expected for HIV-1 particles observed by AFM, TEM or by other techniques (25-27). Anti-gp120 Abs produced a right-shift or enlarged only the ~500 nm D_H species diffusing in virus media, suggesting the presence of HIV env proteins on them (Fig. 1G, 2H). Filtration with 0.2 μm filters dispersed the ~ 500 nm D_H species into smaller particles, but these particles were able to reassemble over time to nearly the same D_H and intensity of the original species (Fig. 3). The re-clustering was prevented by antibodies binding to dispersed virus (Fig. 3H). These combined observations suggest that HIV-1 is present in solution as thermodynamically stable clusters which can be reversibly dispersed. The occurrence of HIV-1 clustering was not affected by the dilution of virus media with PBS or serum, and on whether the virus was produced in epithelial HEK 293T cells or in native virus producer cells such as macrophages or T-cells (Suppl. Fig.1B, 2,3).

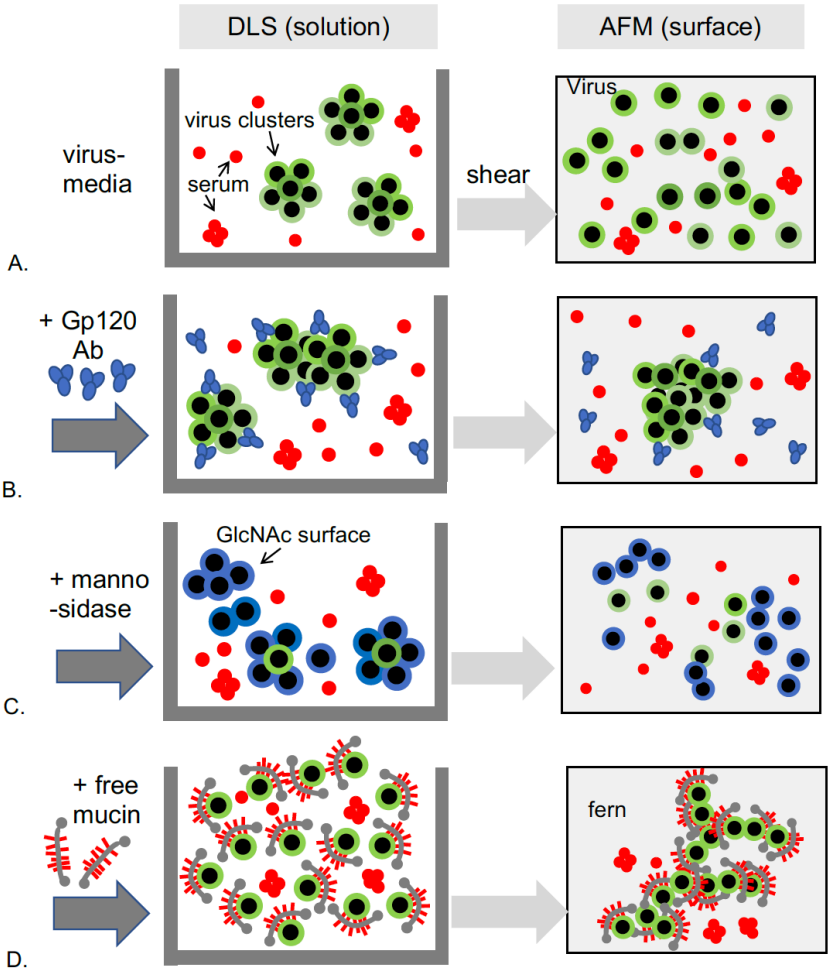

Figure 9: Schematic summarizing how HIV-1 clusters in solution are affected by surface distortion and addition of Abs, mannosidase, and mucin, as seen with both solution-based DLS and surface-based AFM imaging studies. How virus dispersion by filtration modifies this behavior is not shown in the schematic.

Smaller particles in the size range of ~50 nm were also observed in AFM preparations of virus media and in negatively stain TEM imaging. DLS, however, did not show a significant increase in the ~50 nm D_H peak in virus media and these particles were not clearly distinguishable in all sample preparations. It remains uncertain if the presence of these particles was due to stock variation or sample handling during imaging. Previous reports have suggested the presence of similar smaller particles accompanying HIV-1 particles detected using TEM (28, 29).

There have been tangential mentions of HIV-1 aggregation in literature, sometimes attributed as an artifact of virus pelleting during ultracentrifugation (26, 28, 30). Nonetheless, our study did not include purifying the virus with ultracentrifugation on sucrose gradient, and care was given to deconvolute the contribution from serum proteins in media. Our DLS findings suggest that the HIV-1 clustering is a natural of the virus in solution, and it is the stable form. Aggregation in several viruses has been reported, but these aggregates are typically suggested as induced

by extraneous compounds such as mucin or fibrin, or by entrapment within membrane vesicles or endosomes (18,19). Our study does not imply such extraneous compounds to be contributing to HIV-1 clustering. The reversibility of the HIV-1 clustering further rules out the possibility that the aggregates are micro-vesicles of virus or exosomes, since the latter are not expected to reassemble after being sheared apart (31). There have been reports of HIV-1 being retained as aggregates on cell surfaces by tethering proteins from the cell membrane. These tetherins latch on to the membrane of budding out viruses and prevent their release from the cell wall (32). Wild type HIV, however, has proteins that cleave Tetherin bridges and prevent cell-surface accumulations of the virus (33). It is therefore unlikely that the clusters seen in solution are coming from these surface-tethered HIV-1. A DLS study that looked at Ab-induced aggregation of nearly 10 strains of HIV virus showed most of its baseline viruses having D_H between 200 nm and several microns, which indicates that others have also noted aggregated HIV-1 using DLS (31). Another imaging study observed that HIV-1 did not uniformly infect lymphocytes in culture (26). Most viruses were concentrated on few lymphocytes, and large number of lymphocytes did not have virus on them (26). Such uneven infection can be expected if clusters of viruses are interacting with the cells. An early TEM study also mentions that gentle homogenization releases clumps of HIV-1 in solution, though this study suggested the HIV clumps were likely aggregated by extraneous material like glycoproteins (30).

The surface of the virus clusters appears to be coated with high mannose glycans and removal of the mannose partly decreased the size of the clusters (Fig. 5A). The texture and shape of HIV-1 changed with mannose removal and the particles adsorbed on mica in non-random fashion (Fig. 5F, G). It is possible that the removal of mannose and exposure of GlcNAc, a hydrophobic sugar, changes the way HIV-1 adsorbs on an AFM surface. At present, our data is suggesting that mannosidase treatment is only removing the high-mannose glycans on the surface of the clusters because of restricted access to viral surfaces within the cluster, and therefore not completely dispersing the HIV-1 clusters. Mannosidase treatment of filtered and therefore dispersed virus, however, does confirm complete loss of clustering with mannose removal (Suppl. Fig. 7).

Monitoring the viral clusters with DLS shows how HIV clustering limits access of lectins, glycosidases, and antibodies to all surfaces of the virus. Current thought is that Abs aggregate virus multiple-fold only within a small range of concentration where the concentrations of virus and antibody favor inter-virus binding by Ab (31). However, our studies indicates that HIV-1 is aggregated to start with, and that Abs stabilize existing HIV clusters to make them less prone to shearing apart, even if they do not promote large-scale aggregation. Interestingly Abs bound to free viruses do not aggregates confirming that moieties on the gp120 env of the virus are inducing the clustering effect.

The observation that HIV-1 diffuses in ~500 nm packages is interesting because particles > 100 nm are known to preferentially accumulate in the lymphatic region, where cells that HIV-1 targets are also located (34). The cluster organization also has an interesting implication for Ab recognition and neutralization of the virus. In order to neutralize the virus, Abs bind near regions critical for host entry and render them inactive. With HIV-1 packaged into clusters, many of the viral surfaces become inaccessible to Ab binding. In other words, there can always be

un-neutralized viral surfaces within the clusters that can interact with cells when the clusters are reversibly dispersed. The shear reversibility of HIV clustering also opens a new perspective on how fluid shear in blood vessels and the filtration through capillaries will influence HIV-1 distribution through the body.

DLS as a tool for profiling terminal sugars on mixtures with different hydrodynamic sizes: It was found that virus and serum had clear and separable signals in DLS, which were distinguishable with the extraction methodologies of both in-house (21) and instrument (Malvern Zetasizer) software (Fig. 1B,C). Lectin binding/agglutination would increase the size of the diffusing species, and since virus and serum contribute to different regions of the DLS curve, the change in DLS curves following lectin addition can be used to qualitatively check the presence of a terminal sugar on virus or serum. For instance, binding/agglutination of serum alone would be detected as right-shifting (i.e., increasing D_H) of the entire control media and of serum-contributing region of the virus media (i.e., upper reaches of the correlation curve and first two D_H peaks of histogram). (Fig. 1). On the other hand, entities that only bind virus would only right-shift the virus-contributing region of virus media DLS curves (lower region of correlogram and latter peak in D_H histogram) (Fig.4). Lectins for galactose and GlcNAc did not shift the correlation curves of both serum and virus, indicating these sugars were not present in sufficient amounts to give detectable lectin-aggregation signal with their lectins. Lectins for SA (WGA, SNA, and MAA) and Ca ions aggregated only the serum and not virus. ConA, the lectin for mannose, aggregated virus extensively and serum to some extent. The terminal sugar profile of serum is consistent with reports that the principal components of serum-fetuin, serum albumin, and transferrin- are rich in SA (35-37). and with reports that Ca ions bind fetal bovine serum proteins (38). The terminal sugar profile on HIV-1 is consistent with reports that the virus has majority high-mannose glycans irrespective of which cell it is produced in (13). While DLS-based glyco-profiling is not quantitative and identifies only the terminal sugars that are present in amounts sufficient to be aggregated by lectins, it is simple, rapid, and cost-effective compared to profiling with glyco-arrays and mass-spectroscopy and can be accomplished in a single step without cleaving glycans. Moreover, serum proteins do not have to be separated from the virus, and the glycans on intact virus can be distinguished from those shed into solution. For effective DLS glyco-profiling, however, a control solution containing all solution components, but virus is needed to ensure that the non-virus components are not aggregating the lectins. In our case this was achieved by using control media with serum. Also, we observed that large-scale indiscriminate aggregation occurred when Ca ions were added to media solutions diluted with certain PBS brands at pH > 7. Our studies were performed at pH 6.5, and in general we recommend doing pH and control checks against such aggregation artifacts. Also, since culture media itself has Ca ions in it, we did not find it necessary to supplement additional Ca ions for lectin activity unless the media was diluted to large extents with PBS. For glyco-profiling with DLS, the virus solution should be in dilute regime. The hydrodynamic sizes in DLS are determined from the diffusion speed of the species, and any decrease in diffusion speed is mapped to an increase in the size of the species. Therefore, if the species is not in the dilute regime, its diffusion speed can be lowered by crowding efforts and interpreted as an increase in particle size. Finally, DLS-based glyco-profiling tends to work better with lectins that agglutinate as opposed to lectins that coat, and in the solution conditions that favor lectin agglutination.

Free mucin molecules disperse HIV clusters: While lectins, antibodies, and mannosidases did not disperse the viral clusters, free mucin molecules from porcine gastric mucin did. When virus was added to a solution of free mucin molecules, the signal due to viral clusters disappeared and instead only one diffusion size slightly similar to free mucin and single virus was present. However, there was no marked increase in the scattering intensity at the new size (i.e., the total volume of scattering species did not increase with the addition of viral clusters to mucin), raising the possibility that these newly diffusing species were single viruses coated with collapsed mucin. The mucin dispersal of HIV-1 suggests a new interpretation for how mucin inactivates the virus. Multiple studies noted that the addition of mucin (PGM, breast milk, salivary) to HIV-1 reduces the latter's ability to infect cells (39, 40). However, it has been thought that the mucin molecules aggregated the virus, therefore making it unavailable for infecting cells (41). Our studies suggest that in the case of HIV-1, which is clustered to start with, free mucin molecules break the virus clusters and possibly reduce infectivity. The trapping of HIV by mucin molecules could also be a reason why HIV incubated with mucin is not effective in infecting cells, whereas cells incubated with mucin can be infected by viruses (42). SEM images by other researchers show single particles of HIV virus in mucin, which is consistent with our finding that mucin disperses HIV-1 clusters (41).

Dilute solutions of PGM molecules adsorbed on AFM surface as sparse networks. However, when HIV-1 clusters were added to the mix, the inter-mucin interactions that lead to networked adsorption were lost and the virus+mucin solution adsorbed as fern fractals instead. The loss of the inter-mucin interactions that develop when mucin molecules adsorb on a surface suggests that virus and mucin interact in ways that prevent normal mucin-mucin interactions. No viral clusters were detected in the fern structure, which is consistent with the DLS data showing that mucin disperses viral clusters. The AFM phase texture of the virus surface matched that of mucin, suggesting the virus comprising the fern structure was covered with mucin. Fern crystallites or arborization of cervical mucin upon drying are used clinically to diagnose the increased penetration state of cervical mucin that occurs during ovulation and infection (43-46). At present, it is unclear what causes the mucin to switch to forming fern patterns in the presence of HIV-1.

On the other hand, it appears the mucin molecules were favoring the aggregation of serum proteins, which could explain why serum increases the viscosity of mucin solution (47).The dispersion of HIV clusters by mucin was found to be relatively strong, even when the clusters were stabilized by Abs. Our studies on the interaction between HIV and Abs focused on one type of anti-gp120 Ab (goat, polyclonal), and it is possible that the results may not be fully applicable to other types of HIV Abs with different binding epitopes. Nevertheless, this study adds complexity to strategies that seek to trap HIV-1 in vaginal mucus using Abs, Abs may not be able to bind and aggregate HIV-1 particles that are covered with mucin but can bind to HIV-1 particles that escape the mucin coating.

CONCLUSION: The present study reports that mannose-rich HIV virus is present in culture media as clusters, which can be dispersed by filtration shear but can reassemble back after shear is removed. Antibodies appear to stabilize HIV-1 clusters, but they also prevented them from re-clustering. HIV clustering is reduced by removal of

terminal mannose sugars, though viral clustering appears to reduce glycosidase access to their surfaces. Lectins similarly interact with only the surface of the clusters without dispersing them, whereas mucin molecules effectively disperse the HIV clusters. The network architecture of mucin changes to ferning or arborization pattern in the presence of virus, similar to what is seen in cervical mucus during ovulation. Mucin molecules can also disperse HIV clusters stabilized by antibodies. The ability to form reversible clusters provides HIV-1 with the opportunity to temporarily conceal their viral surfaces from glycosidases, antibodies, and lectins in solution, and then release them for infecting cells when exposed to mechanical shear cues. The findings of this study offer a new perspective on how mucin might be interacting with HIV-1 by dispersing viral clusters.

AKNOWLEDGEMENTS: AKNOWLEDGEMENTS: The work was supported by NSF grant # 2000175 (PLC and SN) and NIH grants R03AI167762 (PLC), 1R01HL125005 (SN), 5U54MD007597 (SN) and P30 AI117970 grant from the District of Columbia Center for AIDS Research an NIH funded program (to SN). We acknowledge Dr. Christine Brantner and George Washington University Imaging Center for TEM assistance. The authors thank Dr. James Mitchell for use of facilities, Ms. Anjolaoluwa Bamtefa for assistance with TEM imaging. We thank the DC CFAR team of Dr. Seble Kassaye, Dr. Mark Burke, and Dr. Alberto Bosque for insightful discussions, and Dr. John Hanover and group for critical feedback. We thank NIH AIDS Research and Reference Reagent Program for pHEF-VSVG expression vector (courtesy of Dr. Lung-Ji Chang) and pNL4-3.Luc.R-E- (courtesy of Dr. Nathaniel Landau).

LEGENDS:

Figure 1: HIV-1 clusters in virus media: [A] 'Virus media' refers to clarified culture media from HEK 293T cells producing virus after transfection with plasmids for replication-deficient provirus and Gp120 envelop proteins. [B] DLS correlation curves of virus media and control media (DMEM with FBS) showing significant contribution from serum proteins to both curves. Region of FBS contribution to virus media DLS curve is circled. [C] Virus and serum contributions to the virus media DLS curve are relegated to the upper and lower regions of the curve. [D] Anti-gp120 Ab right-shifts or aggregates the lower region of the virus media DLS curve, confirming that HIV-1 particles are present in the larger diffusing species there. [E] Abs not specific to HIV-1 do not shift virus media DLS curve. [F] Histogram of the hydrodynamic diameters (D_H) showing the virus media has the ~10 and ~50nm peaks from FBS or serum that are also present in control media. Additionally, a larger D_H peak appears in virus media likely from virus clusters diffusing in solution. [G] Anti-gp120 Abs increase the size of the larger D_H peak in virus media indicating that it is contributed by HIV-1 particles.

Figure 2: Imaging of particles in HIV-1 virus media: [A] AFM of control media shows serum proteins in the phase image (top), but which are not apparent in corresponding height image (bottom) having color bar spanning 13 nm. [B] AFM of virus media showing serum and virus in phase image (top) but with the non-serum particles alone highlighted in the color map of the height image (bottom). There are ~40 nm (arrow) and ~80 nm (stars) particles appearing in virus media. [C] Zoomed-in phase (top) and height (bottom) image highlighting the ~80nm (star) and ~40nm (arrow) particles appearing in virus media. In one instance, the ~40nm particle appears to be breaking off the 80nm particles (broken arrow). [D] Particle analysis of multiple AFM images showing serum particles with similar height vs. diameter trend in both control and virus media, and that virus media has new contributions from particles >40 nm with different height vs. diameter trends (n = 3 samples). [E] Negatively-stained TEM of virus media showing both ~80nm (star) and ~40nm (arrow) particles. [F] Envelope spikes are seen on ~80nm particles and free viral cones are visible inside and outside the ~50nm particles suggesting that these are both viruses. [G,H] Supplementing virus media with anti-gp120 Abs stabilizes the HIV-1 clusters in solution for being visible in AFM imaging. Larger clusters of ~80nm viral particles are observed in virus media with anti-gp120 Abs.

Figure 3: HIV-1 clusters are reversibly dispersed by filtration: [A] Distribution of population sizes, D_H, in virus media before, immediately after, and after filtration. The ~500nm virus clusters reduces to ~190 nm size in the filtrate immediately after filtration, but over time the clustering recovering. [B] DLS correlation curves showing dispersal of viral clusters immediately after filtration (left-shift of immediate-time filtrate) and the re-clustering of HIV-1 over time (DLS curves of long-time filtrate and unfiltered overlap). [C] Schematic highlighting the reversible shearing and recovery of HIV-1 clusters in filtration. [D] AFM phase image of undisturbed virus media before filtration showing HIV-1 clusters. [E] AFM phase image of virus media immediately after filtration showing HIV-1 viral particles. [F] DLS histogram showing that HIV-1 clusters which are dispersed by filtration into anti-gp120 Ab solution do not re-cluster back. [G] AFM height and phase image of virus dispersed into antibody solution showing dispersed virus covered by Ab like particles.

Figure 4: Glyco-profiling of terminal sugars on serum and HIV-1 populations in virus media: [A] Scaled DLS curves of control and virus media, highlighting that serum and virus contribute to different regions of the virus-media curve. Lectins ECA [B] and LEL [C] did not shift the virus media and control media curve, indicating that terminal galactose and glcNAc are not predominantly present on both populations. Lectins WGA [D], MAA [E], SNA [F], and Ca [G] shifted the control media and the upper regions of the virus media alone, indicating that terminal SA is present on serum but not on virus. Lectin Con A [H] shifted virus media extensively and serum to some extent indicating it is extensively present on the virus contributing to the lower region of the virus media curve.

Figure 5: β-mannosidase treatment of virus media: [A] β-mannosidase cleavage left-shifts the lower region of the DLS curve contributed by virus-clusters. [B] DLS size histograms showing mannosidase treatment to decrease viral clusters from ~500 nm to ~ 200 nm D_H. [C] Mannose lectin Con A aggregates virus media (right-shift) but not mannosidase-cleaved virus media, confirming removal of mannose from cluster surface in the latter. [D] Mannosidase-cleaved virus, but not the uncleaved control virus, is aggregated by WGA confirming surface exposure of either SA or GlcNAc. [E] Mannose-cleaved virus alone is aggregated by GlcNAc lectin LEL, confirming the exposure of GlcNAc residues from glycan core following the mannose removal. [F] ~80 nm viral particles of lower

height are visible in AFM images (right) following mannose removal and GlcNAc exposure. Uncleaved virus is shown for reference (left). [H] Non-random adsorption of mannose-cleaved virus on AFM mica surface.

Figure 6: Characterization of baseline mucin and serum interactions: [A] Different dilutions of porcine gastric mucin solution in PBS showing that the diffusion speed of the mucin molecules does not change with dilution (i.e., curves do not shift) and therefore the mucin molecules are in free state without dominant inter-mucin interactions. [B] Histogram of hydrodynamic diameters (D_H) in solution showing that the solution of free mucin with control media (i.e., serum proteins) has the same population D_H as control media and mucin alone. [C] DLS correlation curves showing that the mucin+control media curve is nearly the sum of the mucin and control media curves, indicating that there is no major interaction with mucin and serum occurring that would change the type of diffusing species. [D] AFM Images of mucin molecules forming networks in AFM surface shown at two different scales. [E] AFM phase image of serum+mucin highlighting distinguishable serum particles present amidst the adsorbed mucin. [F] Particle analysis of serum+mucin AFM images showing that while serum particles in mucin have similar height vs. diameter trends to serum alone, there is a higher sampling of aggregated serum particles when in the presence of mucin. Arrow marks the 50^{th} percentile particle. The higher heights of mucin+serum particles reflect the mucin layer adsorbed below the serum particles.

Figure 7: Mucin disperses HIV-1 clusters: [A] Mucin loaded with virus adsorbs in fern fractal form. [B] Zoomed in image of mucin arborization in the presence of HIV-1. [C-H] AFM height, phase, and height with multicolor map of virus (left) and of virus coated and trapped in mucin. [I] Height profile comparing virus in media and in mucin. [J] DLS histogram showing that the multiple diffusing populations in virus media and in mucin with control media are replaced by a single diffusing species around ~120 nm D_H in the mixture of virus media and mucin. Notably the ~700 nm D_H from virus clusters in virus media is lost. [K] DLS Correlation curve showing the loss of HIV-1 clusters (left shift of virus curve) when mucin is added.

Figure 8: Mucin disperses HIV-1 clusters stabilized by antibodies: [A] DLS Correlation curve showing that mucin disperses (left-shifts) virus clusters stabilized by anti-gp120 Abs. [B] DLS histogram showing the loss of the > 500 nm D_H virus clusters stabilized by anti-gp120 Abs peak when mucin is added. [C] AFM height (top) and phase (bottom) images showing anti-gp120 Abs (left), viral clusters stabilized by anti-Gp120 Abs (middle), and loss of viral clusters when mucin is added to the mix (right).

Figure 9: Schematic summarizing how HIV-1 clusters in solution are affected by surface distortion, and addition of Abs, mannosidase, and mucin as seen with both solution-based DLS and surface-based AFM imaging studies. How virus dispersion by filtration modifies this behavior is not shown in the schematic.

REFERENCES

1. Barré-Sinoussi, F., Chermann, J. C., Rey, F., Nugeyre, M. T., Chamaret, S., Gruest, J., Dauguet, C., Axler-Blin, C., Vézinet-Brun, F., Rouzioux, C., Rozenbaum, W., and Montagnier, L. (1983) Isolation of a T-lymphotropic retrovirus from a patient at risk for acquired immune deficiency syndrome (AIDS). *Science* **220**, 868-871
2. Stamatatos, L., Morris, L., Burton, D. R., and Mascola, J. R. (2009) Neutralizing antibodies generated during natural HIV-1 infection: good news for an HIV-1 vaccine? *Nature Medicine* **15**, 866-870
3. Piguet, V., and Trono, D. (2001) Living in oblivion: HIV immune evasion. *Seminars in Immunology* **13**, 51-57
4. Piacenti, F. J. (2006) An Update and Review of Antiretroviral Therapy. *Pharmacotherapy: The Journal of Human Pharmacology and Drug Therapy* **26**, 1111-1133
5. Broder, S. (2010) The development of antiretroviral therapy and its impact on the HIV-1/AIDS pandemic. *Antiviral Research* **85**, 1-18
6. Walker, B. D., and Burton, D. R. (2008) Toward an AIDS vaccine. *science* **320**, 760-764
7. Maldarelli, F., Kearney, M., Palmer, S., Stephens, R., Mican, J., Polis, M. A., Davey, R. T., Kovacs, J., Shao, W., Rock-Kress, D., Metcalf, J. A., Rehm, C., Greer, S. E., Lucey, D. L., Danley, K., Alter, H., Mellors, J. W., and Coffin, J. M. (2013) HIV populations are large and accumulate high genetic diversity in a nonlinear fashion. *J Virol* **87**, 10313-10323
8. Karlsson, A. C., Deeks Sg Fau - Barbour, J. D., Barbour Jd Fau - Heiken, B. D., Heiken Bd Fau - Younger, S. R., Younger Sr Fau - Hoh, R., Hoh R Fau - Lane, M., Lane M Fau - Sällberg, M., Sällberg M Fau - Ortiz, G. M., Ortiz Gm Fau - Demarest, J. F., Demarest Jf Fau - Liegler, T., Liegler T Fau - Grant, R. M., Grant Rm Fau - Martin, J. N., Martin Jn Fau - Nixon, D. F., and Nixon, D. F. Dual pressure from antiretroviral therapy and cell-mediated immune response on the human immunodeficiency virus type 1 protease gene.
9. Ringe, R., and Bhattacharya, J. (2013) Preventive and therapeutic applications of neutralizing antibodies to Human Immunodeficiency Virus Type 1 (HIV-1). *Ther Adv Vaccines* **1**, 67-80
10. Spencer, D. A., Shapiro, M. B., Haigwood, N. L., and Hessell, A. J. (2021) Advancing HIV Broadly Neutralizing Antibodies: From Discovery to the Clinic. *Frontiers in Public Health* **9**
11. Raska, M., and Novak, J. (2010) Involvement of Envelope-Glycoprotein Glycans in HIV-1 Biology and Infection. *Archivum Immunologiae et Therapiae Experimentalis* **58**, 191-208
12. Seabright, G. E., Doores, K. J., Burton, D. R., and Crispin, M. (2019) Protein and Glycan Mimicry in HIV Vaccine Design. *J Mol Biol* **431**, 2223-2247
13. Bonomelli, C., Doores, K. J., Dunlop, D. C., Thaney, V., Dwek, R. A., Burton, D. R., Crispin, M., and Scanlan, C. N. (2011) The glycan shield of HIV is predominantly oligomannose independently of production system or viral clade. *PloS one* **6**, e23521
14. Mascola, J. R., and Montefiori, D. C. (2003) HIV-1: nature's master of disguise. *Nature Medicine* **9**, 393-394
15. Abeyratne-Perera, H. K., and Chandran, P. L. (2017) Mannose Surfaces Exhibit Self-Latching, Water Structuring, and Resilience to Chaotropes: Implications for Pathogen Virulence. *Langmuir* **33**, 9178-9189
16. Abeyratne-Perera, H. K., Ogarandukun, E., and Chandran, P. (2019) Complex-type N-glycans on VSV-G pseudotyped HIV exhibit 'tough' sialic and 'brittle' mannose self-adhesions. *Soft Matter* **15**, 4525-4540
17. Ogharandukun, E., Tewolde, W., Damtae, E., Wang, S., Ivanov, A., Kumari, N., Nekhai, S., and Chandran, P. L. (2020) Establishing Rules for Self-Adhesion and Aggregation of N-Glycan Sugars Using Virus Glycan Shields. *Langmuir* **36**, 13769-13783
18. Pradhan, S. A.-O., Varsani, A. A.-O., Leff, C. A.-O., Swanson, C. A.-O., and Hariadi, R. A.-O. X. Viral Aggregation: The Knowns and Unknowns. LID - 10.3390/v14020438 [doi] LID - 438.
19. Wallis, C., and Melnick, J. L. (1967) Virus aggregation as the cause of the non-neutralizable persistent fraction. *J Virol* **1**, 478-488
20. Charles, S., Ammosova, T., Cardenas, J., Foster, A., Rotimi, J., Jerebtsova, M., Ayodeji, A. A., Niu, X., Ray, P. E., Gordeuk, V. R., Kashanchi, F., and Nekhai, S. (2009) Regulation of HIV-1 transcription at 3% versus 21% oxygen concentration. *Journal of cellular physiology* **221**, 469-479
21. Chandran, P. L. (2020) Sequential Extraction of Late Exponentials (SELE): A technique for deconvolving multimodal correlation curves in Dynamic Light Scattering. *MRS Advances* **5**, 865-880
22. Goldburg, W. I. (1999) Dynamic light scattering. *American Journal of Physics* **67**, 1152-1160

23. Pecora, R. (2000) Dynamic light scattering measurement of nanometer particles in liquids. *Journal of nanoparticle research* **2**, 123-131
24. Reicin, A. S., Ohagen, A., Yin, L., Hoglund, S., and Goff, S. P. (1996) The role of Gag in human immunodeficiency virus type 1 virion morphogenesis and early steps of the viral life cycle. *Journal of virology* **70**, 8645-8652
25. Stannard, L. M., van der Riet, F. D. S. J., and Moodie, J. W. (1987) The Morphology of Human Immunodeficiency Virus Particles by Negative Staining Electron Microscopy. *Journal of General Virology* **68**, 919-923
26. Kuznetsov, Y. G., Victoria, J. G., Robinson, W. E., Jr., and McPherson, A. (2003) Atomic force microscopy investigation of human immunodeficiency virus (HIV) and HIV-infected lymphocytes. *J Virol* **77**, 11896-11909
27. Darvish, A., Lee, J. S., Peng, B., Saharia, J., VenkatKalyana Sundaram, R., Goyal, G., Bandara, N., Ahn, C. W., Kim, J., Dutta, P., Chaiken, I., and Kim, M. J. (2019) Mechanical characterization of HIV-1 with a solid-state nanopore sensor. *Electrophoresis* **40**, 776-783
28. Hockley, D. J., Wood, R. D., Jacobs, J. P., and Garrett, A. J. (1988) Electron Microscopy of Human Immunodeficiency Virus. *Journal of General Virology* **69**, 2455-2469
29. Chrystie, I. L., and Almeida, J. D. (1988) The morphology of human immunodeficiency virus (HIV) by negative staining. *Journal of Medical Virology* **25**, 281-288
30. Chrystie, I. L., and Almeida, J. D. (1988) Further studies of HIV morphology by negative staining. *Aids* **2**, 459-464
31. Alexander, M. R., Sanders, R. W., Moore, J. P., and Klasse, P. J. (2015) Short Communication: Virion Aggregation by Neutralizing and Nonneutralizing Antibodies to the HIV-1 Envelope Glycoprotein. *AIDS Res Hum Retroviruses* **31**, 1160-1165
32. Perez-Caballero, D., Zang T Fau - Ebrahimi, A., Ebrahimi A Fau - McNatt, M. W., McNatt Mw Fau - Gregory, D. A., Gregory Da Fau - Johnson, M. C., Johnson Mc Fau - Bieniasz, P. D., and Bieniasz, P. D. Tetherin inhibits HIV-1 release by directly tethering virions to cells.
33. Neil, S. J., Zang, T., and Bieniasz, P. D. (2008) Tetherin inhibits retrovirus release and is antagonized by HIV-1 Vpu. *Nature* **451**, 425-430
34. Zhang, Y.-N., Lazarovits, J., Poon, W., Ouyang, B., Nguyen, L. N. M., Kingston, B. R., and Chan, W. C. W. (2019) Nanoparticle Size Influences Antigen Retention and Presentation in Lymph Node Follicles for Humoral Immunity. *Nano Letters* **19**, 7226-7235
35. Cartellieri, S., Hamer, O., Helmholz, H., and Niemeyer, B. (2002) One-step affinity purification of fetuin from fetal bovine serum. *Biotechnology and Applied Biochemistry* **35**, 83-89
36. Sun, S., Hu, Y., Jia, L., Eshghi, S. T., Liu, Y., Shah, P., and Zhang, H. (2018) Site-Specific Profiling of Serum Glycoproteins Using N-Linked Glycan and Glycosite Analysis Revealing Atypical N-Glycosylation Sites on Albumin and α-1B-Glycoprotein. *Analytical Chemistry* **90**, 6292-6299
37. Grünewald, S., Matthijs, G., and Jaeken, J. (2002) Congenital Disorders of Glycosylation: A Review. *Pediatric Research* **52**, 618-624
38. Suzuki, M., Shimokawa, H., Takagi, Y., and Sasaki, S. (1994) Calcium-binding properties of fetuin in fetal bovine serum. *J Exp Zool* **270**, 501-507
39. Mall, A. S., Habte, H., Mthembu, Y., Peacocke, J., and de Beer, C. (2017) Mucus and Mucins: do they have a role in the inhibition of the human immunodeficiency virus? *Virology Journal* **14**, 192
40. McQuaid, I. K., Dorfman, J. R., and Mall, A. S. (2021) The comparative inhibitory potency of salivary mucins against human immunodeficiency virus type 1. *Virology* **553**, 1-8
41. Bergey, E. J., Cho, M.-I., Hammarskjöld, M.-L., Rekosh, D., Levine, M. J., Blumberg, B. M., and Epstein, L. G. (1993) Aggregation of Human Immunodeficiency Virus Type 1 by Human Salivary Secretions. *Critical Reviews in Oral Biology & Medicine* **4**, 467-474
42. Malamud, D., Nagashunmugam, T., Davis, C., Kennedy, S., Abrams, W., Kream, R., and Friedman, H. (1997) Inhibition of HIV infectivity by human saliva. *Oral Diseases* **3**, S58-S63
43. Abou-Shabanah, E. H., and Plotz, E. J. (1957) A biochemical study of the cervical and nasal mucus fern phenomenon. *American Journal of Obstetrics and Gynecology* **74**, 559-568
44. Hilgers, T. W., and Prebil, A. M. (1979) The Ovulation Method—Vulvar Observations as an Index of Fertility/Infertility. *Obstetrics & Gynecology* **53**
45. Ullery, J. C., Livingston, N., and Abou-Shabanah, E. H. (1959) the mucous fern phenomenon in the cervical and nasal smears: a review and current concept of arborization. *Obstetrical & Gynecological Survey* **14**

46. Priya, B. S., Pushpaja, M., and Maruthy, K. (2020) Does the salivary fern pattern determine fertile period in reproductive female? *Clinical Epidemiology and Global Health* **8**, 698-701
47. List, S. J., Findlay, B. P., Forstner, G. G., and Forstner, J. F. (1978) Enhancement of the viscosity of mucin by serum albumin. *Biochemical Journal* **175**, 565-571

SUPPLEMENTARY INFORMATION

Shear-reversible clusters of HIV-1 in solution: stabilized by Abs, dispersed by mucin

Ayobami Ogundiran[1], Tzu-Lan Chang[1], Andrey Ivanov[3], Namita Kumari[3,4], Sergei Nekhai[3,4], Preethi L. Chandran[1,2]

[1] Department of Chemical Engineering, College of Engineering and Architecture

[2] Department of Biochemistry and Molecular Biology, College of Medicine

[3] Center for Sickle Cell Disease, College of Medicine

[4] Department of Medicine, College of Medicine

Howard University, Washington DC

Corresponding author

Preethi L. Chandran, PhD

Associate Professor

Department of Chemical Engineering, College of Engineering and Architecture, Howard University

Department of Biochemistry and Molecular Biology, College of Medicine, Howard University

Address:

1011 LK Downing Hall

2300 6th Street, NW, Howard University

Washington, DC 20059.

Email: preethi.chandran@howard.edu

Phone: 202-806-4595

Keywords: HIV, VSV Gp120 protein, glycosylation, viral aggregation, virus, Dynamic Light Scattering, AFM, high mannose, lectin, mucin

Email: preethi.chandran@howard.edu
Phone: 202-806-4595

Supplement data

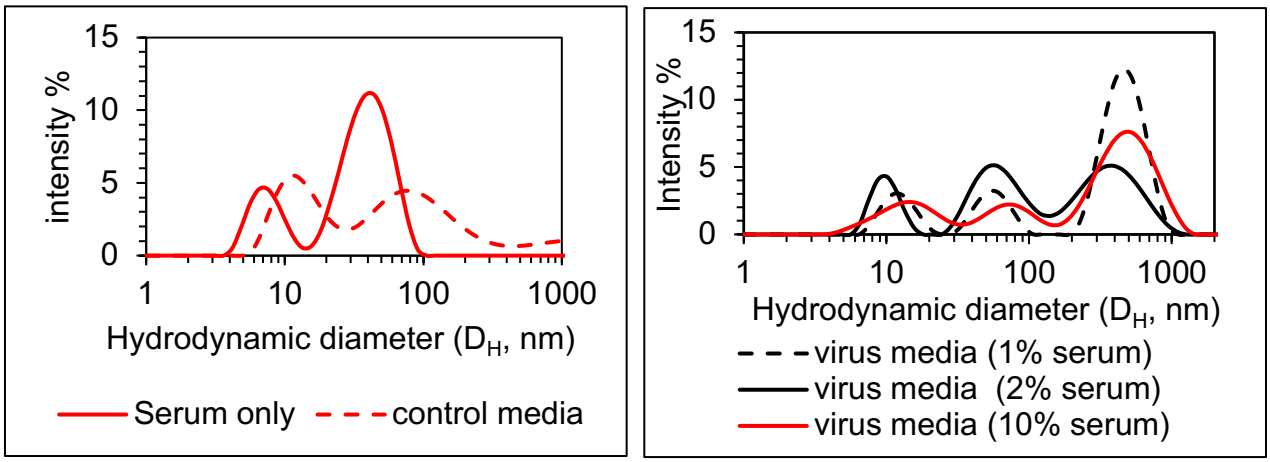

A. B.

Figure S1: The distribution of populations in fetal bovine serum (FBS) and control media. Two population sizes are observed in both solutions. The appearance of viral aggregates was not influenced by the extent of supplementation (vol/vol) % with serum.

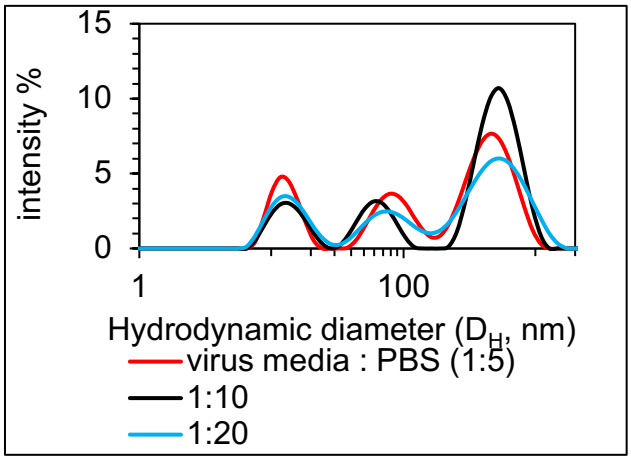

Figure S2: The presence of viral aggregates was not affected by the PBS dilution and has consistent size distribution for serum components and virus clusters.

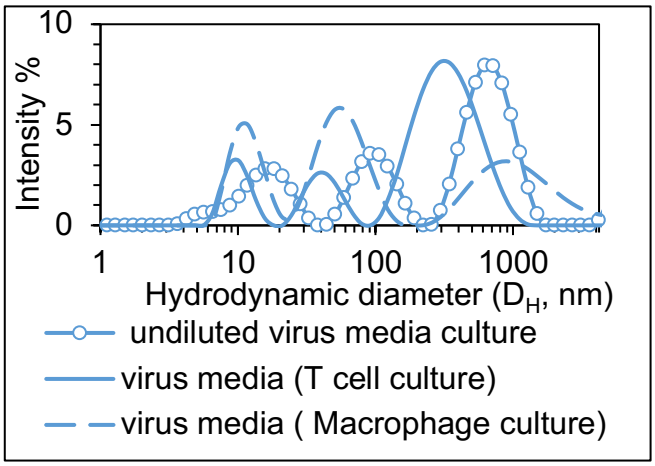

Figure S3: Virus-media containing replication-competent HIV produced from macrophage and T cell cultures also had contribution from > 200 nm particles larger than the size of single HIV-1 diffusing in addition to serum.

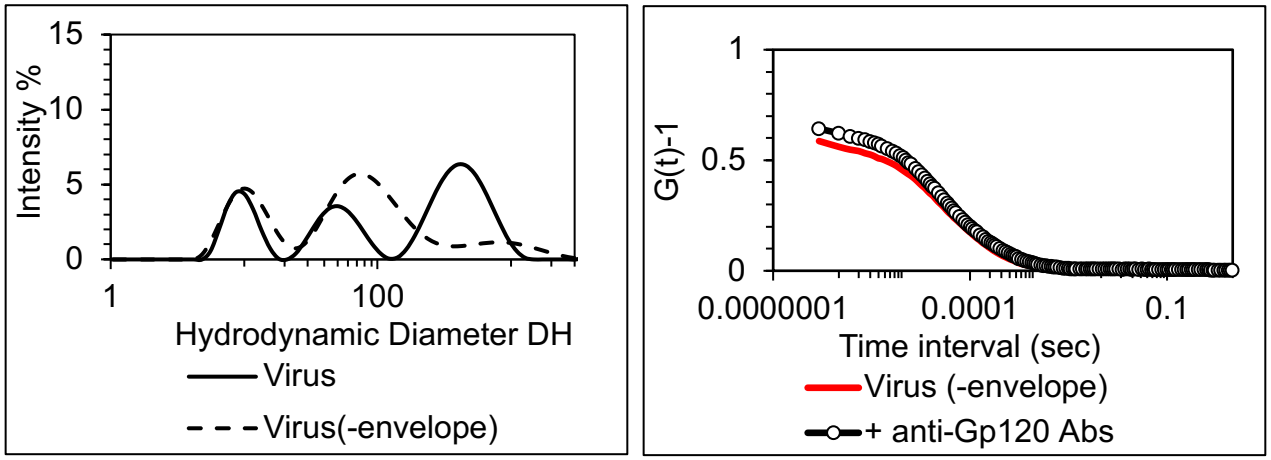

A. B.

Figure S4: Bald virus, i.e., without the envelop protein, did not show viral clusters (D_H > 100nm) such as those observed with virus having gp120 envelop protein (A). The absence of virus clustering in bald virus further confirmed that the envelop protein is involved in the formation of HIV-1 clusters. The addition of anti-gp120 antibodies to bald virus did not increase the size of virus clusters in DLS correlation curves (B), unlike that observed when the antibodies were added to HIV-1 (Fig. 1E).

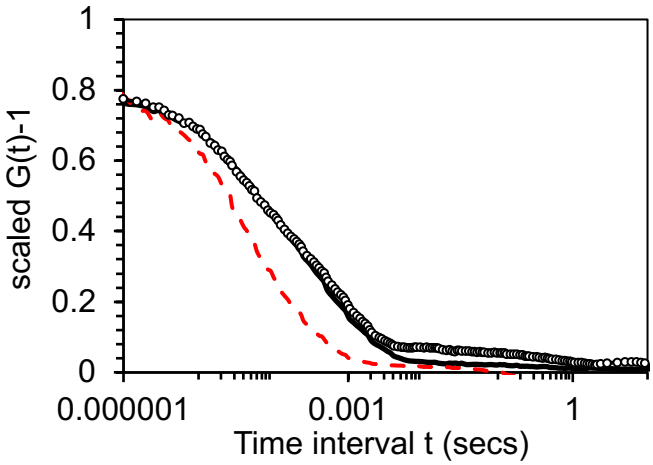

Figure S5: Scaled DLS correlation curves highlighting the complete recovery of virus-media diffusion sizes (i.e., recovery of virus aggregation) after filtration temporarily disperses the virus aggregates.

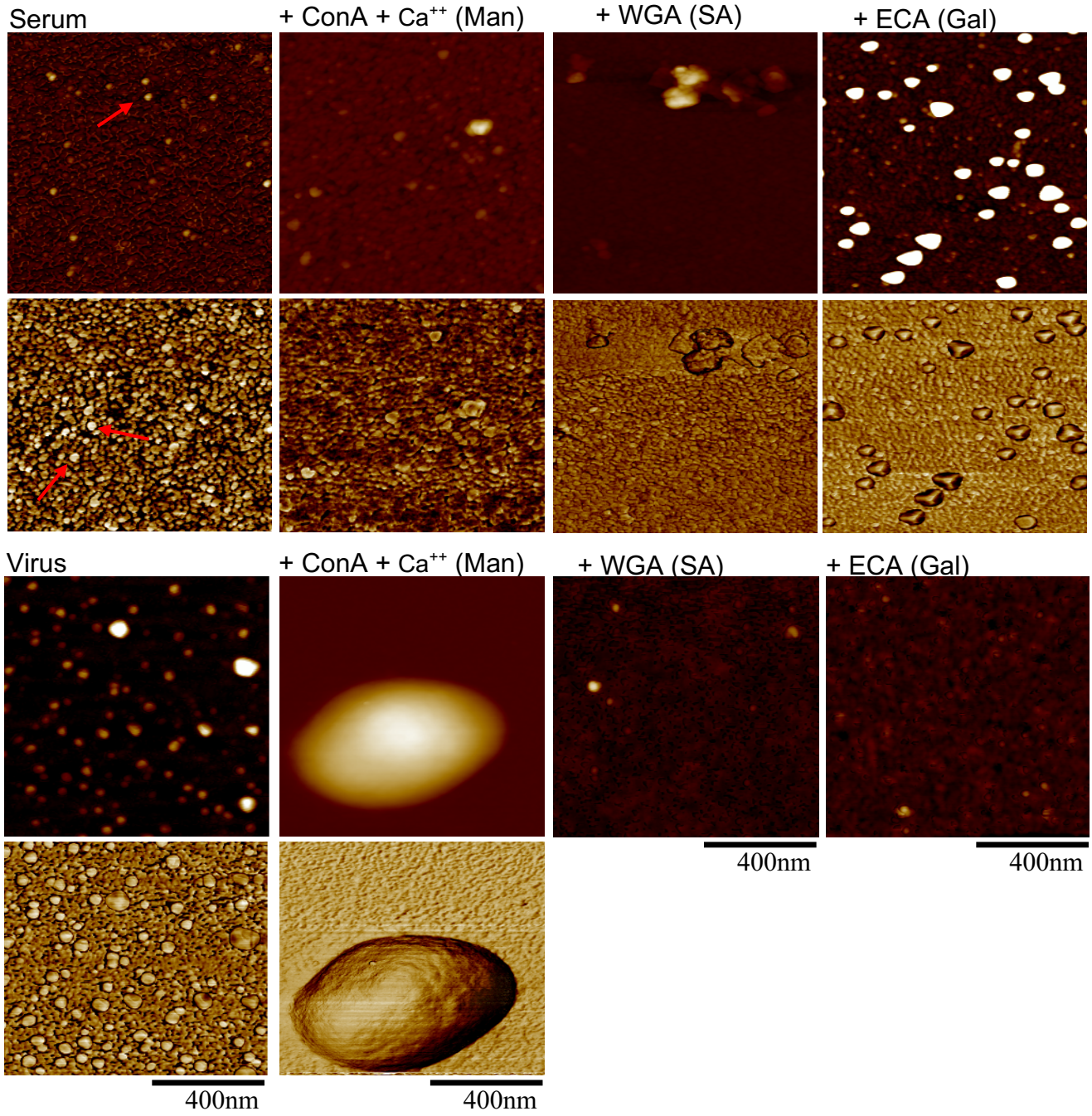

Figure S6: Image of serum and viral agglutination with various lectins using Atomic Force Microscopy shows aggregates when WGA or Ca was added to virus media, but not when ECA or LEL was added, and Con A produced small aggregates of serum proteins but large aggregates with virus-media. Salt crystals were visible in serum + ECA image

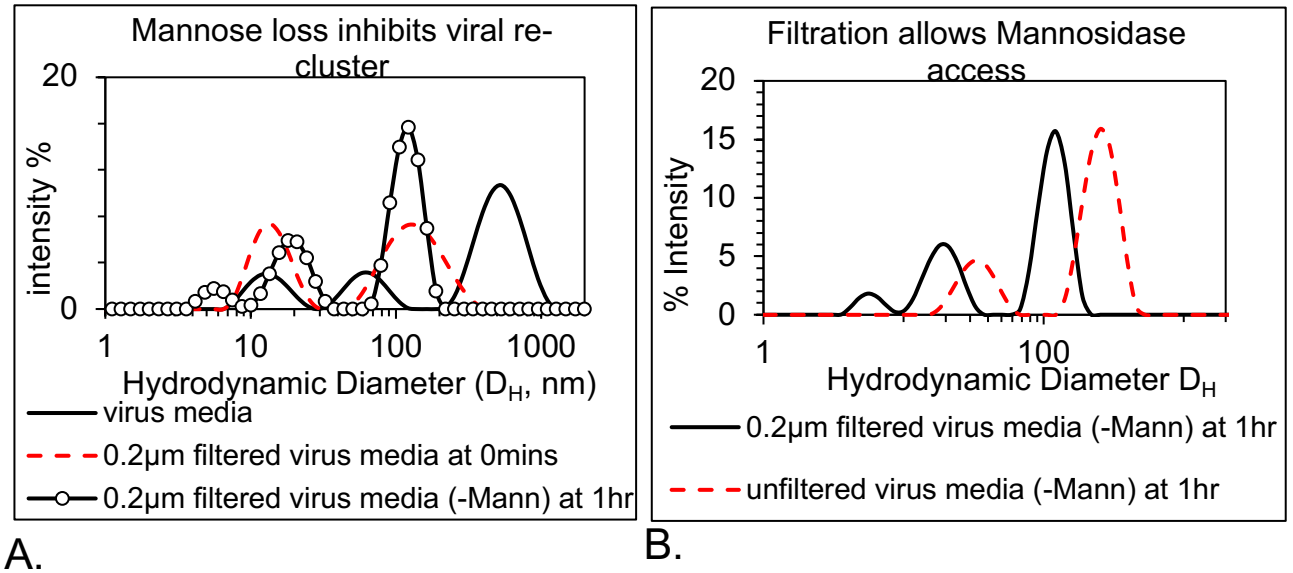

A. B.

Figure S7: Reversible aggregation of HIV-1: Upon filtration, the virus contribution to virus-media in the lower region of the curve shifts leftwards (red arrow) as the clusters disperse. However, over time, the region of virus contribution to the filtered media shifts rightwards (black arrow) indicating recovery of the virus clustering. By 24 hours there is complete recovery of the intensity (i.e., scattering volume) and size of the virus clusters.